








## Article

# Suppression of Ovarian Cancer Cell Proliferation Is Associated with Upregulation of Cell-Matrix Adhesion Programs and Integrin- $\beta$ 4-Induced Cell Protection from Cisplatin

Sadaf Farsinejad <sup>1</sup>, Daniel Centeno <sup>1</sup>, Jan Savas-Carstens <sup>2</sup>, Teagan Polotaye <sup>1</sup> , Tonja Pavlovič <sup>1</sup> , Pouria Babvey <sup>3</sup>, Taru Muranen <sup>4,5</sup> , Cezary Miedziarek <sup>6</sup>, Piotr Jasiński <sup>7</sup>, Elżbieta Dziabaszewska <sup>7</sup>, Mikołaj Piotr Zaborowski <sup>6,8</sup> , Pek Yee Lum <sup>9</sup> , Laura A. Martin <sup>2,\*</sup>  and Marcin P. Iwanicki <sup>1,\*</sup> 

<sup>1</sup> Department of Chemistry and Chemical Biology, Stevens Institute of Technology, Hoboken, NJ 07030, USA; sfarsine@stevens.edu (S.F.); dcenteno@stevens.edu (D.C.); rpolotay@stevens.edu (T.P.); tpavlovi@stevens.edu (T.P.)

<sup>2</sup> New York Stem Cell Foundation Research Institute, New York, NY 10019, USA; jsavascarstens@nyscf.org

<sup>3</sup> School of Systems and Enterprises, Stevens Institute of Technology, Hoboken, NJ 07030, USA; pbabvey@stevens.edu

<sup>4</sup> Department of Medicine, Cancer Research Institute, Beth Israel Deaconess Medical Center, Boston, MA 02215, USA; tmuranen@bidmc.harvard.edu

<sup>5</sup> Harvard Medical School, Boston, MA 02115, USA

<sup>6</sup> Department of Gynecologic Oncology, Chair of Gynecology, Poznań, University of Medical Sciences, 33 Polna Street, 60-535 Poznań, Poland; 77056@student.ump.edu.pl (C.M.); mzaborowski@ump.edu.pl (M.P.Z.)

<sup>7</sup> Department of Pathology in Obstetrics and Gynecology Hospital, Poznań, University of Medical Sciences, Polna 33, 60-535 Poznań, Poland; edziabaszewska@gpsk.ump.edu.pl (E.D.)

<sup>8</sup> Institute of Bioorganic Chemistry, Polish Academy of Sciences, Noskowskiego 12/14, 61-704 Poznań, Poland

<sup>9</sup> Auransa, Palo Alto, CA 94303, USA; pek@auransa.com

\* Correspondence: landresmartin@nyscf.org (L.A.M.); miwanick@stevens.edu (M.P.I.)



Academic Editor: Ugo Cavallaro

Received: 11 February 2025

Revised: 12 April 2025

Accepted: 21 April 2025

Published: 27 April 2025

**Citation:** Farsinejad, S.; Centeno, D.; Savas-Carstens, J.; Polotaye, T.; Pavlovič, T.; Babvey, P.; Muranen, T.; Miedziarek, C.; Jasiński, P.; Dziabaszewska, E.; et al. Suppression of Ovarian Cancer Cell Proliferation Is Associated with Upregulation of Cell-Matrix Adhesion Programs and Integrin- $\beta$ 4-Induced Cell Protection from Cisplatin. *Cancers* **2025**, *17*, 1472. <https://doi.org/10.3390/cancers17091472>

**Copyright:** © 2025 by the authors. Licensee MDPI, Basel, Switzerland. This article is an open access article distributed under the terms and conditions of the Creative Commons Attribution (CC BY) license (<https://creativecommons.org/licenses/by/4.0/>).

**Simple Summary:** Ovarian Cancer (OC) cells can become resistant to chemotherapy, but it is unclear how their ability to attach to the surrounding environment affects this process. First, we analyzed patient databases and found that when integrin beta 4, a protein important for cell attachment, was high, the genes driving cell growth were lower, and vice versa. Next, we blocked cell growth with a drug called Palbociclib and unexpectedly saw that integrin beta 4 increased, reducing the cells' response to Cisplatin (a common chemotherapy). We confirmed these findings in OC cell lines and in patient-derived samples. Moreover, over-expressing integrin beta 4 caused cells to grow more slowly yet become more resistant to Cisplatin. These findings highlight how integrin beta 4 and the surrounding cell environment shape both cancer growth and treatment response, suggesting new ways to improve OC therapies.

**Abstract: Background:** The role of extracellular matrix adhesion components in modulation of the treatment sensitivity of ovarian cancer (OC) cells is not well understood. **Methods and Results:** Analysis of ovarian cancer TCGA gene expression datasets revealed an inverse correlation between genes involved in cell-cycle progression and extracellular matrix interactions, including laminin-binding receptor integrin  $\beta$ 4, a major component of extracellular matrix adhesion. Gene ontology analysis also showed that in patient populations with low *ITGB4* expression, cell cycle-related programs were activated, while in populations with high expression of *ITGB4*, the activation of these cell cycle programs was lower. Suppression of proliferation with the CDK4/6 inhibitor Palbociclib stimulated integrin  $\beta$ 4 expression and induced protection against Cisplatin in cells naturally expressing low levels of integrin  $\beta$ 4. Additionally, ovarian cancer patient-derived organoids showed reduced Cisplatin sensitivity when pretreated with Palbociclib. Our data also showed that integrin  $\beta$ 4 overexpression decreased ovarian cancer cell proliferation and at the same time,

attenuated Cisplatin response. **Conclusions:** In summary, our investigations support the idea that integrin  $\beta 4$ , and likely its matrix ligands, play critical roles in the regulation of cellular growth and the chemoresistance of ovarian cancer cells.

**Keywords:** integrins; integrin  $\beta 4$ ; proliferation; ECM; ovarian cancer; cisplatin

## 1. Introduction

Recent characterization of the transcriptomic landscapes of ovarian cancer (OC) revealed an association of markers of enhanced proliferation with long-term survival [1]. These results suggested that the evolution of low-proliferating OC cell clones might be associated with the activation of growth-suppressing mechanisms that could restrict the actions of current therapies. We have recently published that chemotherapy-recovered ovarian tumors are associated with laminin deposition, and, in culture, elevation of predominantly laminin-containing extracellular matrix (ECM) deposition suppressed cell proliferation and the formation of OC outgrowths [2,3]. These studies raised an important question of whether ECM receptors (integrins) modulate the therapy response of slowly proliferating cancer cells.

Integrins are the cell surface  $\alpha\beta$  heterodimer glycoprotein molecules that bind ECM and transduce mechanical and biochemical signals from extracellular space into cells [4]. In vertebrates, the combinatorial  $\alpha\beta$  complexity yields twenty-two distinct integrin dimers that can interact with various ECM components, including collagens and laminins [5]. For instance, the integrin  $\beta 4$  subunits can associate with the integrin  $\alpha 6$  subunits to form the laminin-binding receptor [6]. Prior studies provide data that starvation of epithelial cells, which causes cell cycle arrest, induces integrin  $\beta 4$  expression and integrin  $\beta 4$ /laminin-dependent survival [7]. Furthermore, recent work has emphasized the significant role of integrin  $\beta 4$  in shaping the tumor microenvironment (TME) and contributing to anti-cancer drug resistance. By binding laminin and forming specialized adhesion complexes, integrin  $\beta 4$  can sustain pro-survival signaling cascades, including PI3K/Akt and NF- $\kappa$ B, thereby helping cancer cells endure therapeutic stress [6,8]. In multiple epithelial malignancies, including breast cancer, integrin  $\beta 4$  is implicated in establishing slow-cycling, quiescent cell populations that are less sensitive to DNA-damaging agents, including Cisplatin and the anthracycline Epirubicin [8]. Moreover, these integrin  $\beta 4$ -rich tumor cells can actively remodel their local ECM, cultivating a TME that supports enhanced cell survival and potentially impacts immune interactions [2,3]. This phenomenon of growth arrest coupled with enhanced therapy tolerance raises questions about the role of integrin  $\beta 4$  upregulation in altering the sensitivity of OC to Cisplatin and other chemotherapeutics. Although well characterized in breast cancer, where it is associated with therapy resistance and quiescent cell populations, integrin  $\beta 4$ 's impact on OC is less defined. This is particularly significant given the prevalent development of chemoresistance in OC.

In this study, we used a combination of The Cancer Genome Atlas (TCGA) data analysis of ovarian serous cystadenocarcinoma, OC cell cultures, and RNA sequencing of growth-arrested OC cells to identify integrin  $\beta 4$  as a critical modulator of cell proliferation and Cisplatin sensitivity. Our data are consistent with the model whereby laminin-binding receptors support the evolution of slowly proliferating, treatment-resistant ovarian cancer cell clones.

## 2. Materials and Methods

### 2.1. Cell Culture

Our study used the following OC cell lines: HEYA8, KURAMOCHI, OVCAR4, OV-90, CAO3, TYK-nu, OVCAR3, OVSAHO, and RMUGS. KURAMOCHI, OVCAR4, OV-90, and OVCAR3 cells were kindly provided by Dr. Denise Connolly (Fox Chase Cancer Center, Philadelphia, PA, USA), HEYA8 cells were a kind gift from Dr. Sumegha Mitra (Washington University School of Medicine, St. Louis, MO, USA), TYK-nu, OVSAHO, and RMUGS cells were provided by Dr. Joan Brugge (Harvard Medical School, Boston, MA, USA), and CAO3 cells were purchased from the American Type Culture Collection (ATCC, Manassas, VA, USA). Each cell line was cultured under optimized conditions to support their growth and maintenance. KURAMOCHI, OVCAR4, OV-90, and OVCAR3 cells were maintained in DMEM/F12 medium (Gibco, Waltham, MA, USA) containing 10% heat-inactivated fetal bovine serum (HI-FBS; Sigma-Aldrich, Burlington, MA, USA) and 1% penicillin-streptomycin (Gibco, Waltham, MA, USA). HEYA8, TYK-nu, OVSAHO, RMUGS, and CAO3 cells were cultured in a 1:1 mixture of MCDB 105 (Sigma-Aldrich) and Medium 199 (Gibco), supplemented with 5% HI-FBS and 1% penicillin-streptomycin. All cells were grown in a humidified 37 °C incubator with 5% CO<sub>2</sub> and passaged at approximately 80% confluence using 0.25% trypsin-EDTA (Gibco). Mycoplasma testing was routinely performed every three to six months using the Uphoff and Drexler method [9].

### 2.2. 3D Spheroid Formation and Matrigel Supplementation

To generate 3D spheroids, 100 cells per well were seeded in a Nunclon Sphera™ round-bottom, ultra-low-attachment 96-well plate (Thermo Fisher Scientific, Waltham, MA, USA; #174929). After a quick centrifugation, the plate was incubated overnight so the cells could make their cell–cell adhesions and aggregate into spheroids. The next day, we allowed the plate to reach the room temperature. The Matrigel was thawed on ice at 4 °C overnight and remained on ice to prevent premature gelation. We kept all tools and pipette tips cold (pre-cooled at −80 °C). We added the Matrigel to a pre-cooled culture medium to make a concentration of 4% (*v/v*). Then, this mixture was added to the spheroids, making a final concentration of 2% (*v/v*). Subsequently, the spheroid plate was allowed to settle at room temperature before returning it to the cell culture incubator. This step ensured even distribution of Matrigel around spheroids before forming a gel. Spheroid cultures were maintained under normal culture condition for five to seven days after seeding, allowing for spheroid growth and potential outgrowth formation.

### 2.3. Cell Proliferation Analysis

Cell proliferation in ovarian cancer cell lines was evaluated using the alamarBlue assay (Invitrogen, Carlsbad, CA, USA, #DAL1025) which measures metabolic activity of the cells, which reflects cell proliferation. Each cell line was seeded in 10 wells of a 96-well plate, with 5 wells for the initial time point (Time 1) after overnight attachment, and another 5 wells for 48 h after the initial read (Time 2). The assay involves adding alamarBlue reagent to each well, as per the manufacturer's instructions. The fluorescence was measured at excitation of 560 nm and emission of 590 nm using a SpectraMax i3x Microplate Reader (Molecular Devices, San Jose, CA, USA). The fluorescence values were background-subtracted, and results were normalized by dividing the fluorescence values at time 2 by those obtained at time 1 to calculate the relative proliferation rate.

Cell lines engineered for doxycycline-inducible expression of *ITGB4* and its respective controls were seeded in black, ibidi-treated square plates to study the impact of integrin  $\beta 4$  expression on cell proliferation. Both *ITGB4*-expressing and control groups were subjected to doxycycline for equal experimental conditions. Cell proliferation was monitored over

a period of 48 h using an automated fluorescent microscope (BTLEFX, Biotek, Lionheart, Winooski, VT, USA), taking pictures every 2 h. For quantification, ImageJ v1.53 k (National Institutes of Health, Bethesda, MD, USA) software was used, combining automated cell detection with manual verification at the end to ensure accuracy. The proliferation rate was normalized to the initial number of cells so that growth dynamics could be directly compared under controlled conditions.

## 2.4. Patient-Derived Organoids

### 2.4.1. Organoid Derivation and Culture

Organoids were retrieved from the NYSCF ovarian cancer organoid biobank. Organoids were generated from fresh tumor tissue biospecimens obtained from patients diagnosed with ovarian cancer as described previously [10–13]. De-identified tumor material was provided by the NCI Cooperative Human Tissue Network (CHTN). Biospecimens correspond to remnants of tissue material that is removed as part of routine medical care collected in accordance with relevant state and local law. Other investigators may have received specimens from the same tissue specimens. The CHTN's Research Resource identifier (RRID) is SCR\_004446. For organoid derivation, tumor tissue was digested with 0.7 mg/mL collagenase (Sigma C9407) in the presence of 10  $\mu$ M Y27632 (AbMole, cat. No. M1817) at 37 °C for 25–50 min. Next, large undigested tissue fragments were removed by passing the tissue suspension through a 100  $\mu$ m cell strainer. The filtered tissue was then centrifuged at 300 $\times$  g for 5 min. If any red blood cells were observed (red pellet) lysis was performed with red blood cell lysis buffer (Sigma-Aldrich, cat. no. 11814389001) for 3 min at room temperature and again centrifuged at 300 $\times$  g for 5 min. The dissociated tissue pellet was resuspended in ice-cold Cultrex Reduced Growth Factor BME type 2 (R&D Systems, Minneapolis, MN, USA, cat. no. 3533-005-02) and at least 40,000 cells in 25  $\mu$ L droplets were plated into pre-warmed 48-well plates. Droplets were allowed to solidify at 37 °C for at least 30 min. Solidified droplets were then overlaid with ovarian tumor organoid medium containing 10  $\mu$ M Y27632 (AbMole, cat. No. M1817). Organoid medium is composed of Advanced DMEM/F12 (Thermo-Fisher, Fair Lawn, NJ, USA, cat. no. 12634-010), 1 $\times$  GlutaMAX (Gibco Thermo Fisher, Fair Lawn, NJ, USA, cat. no. 2492933), 1 $\times$  penicillin-streptomycin (10,000 U/mL) (Life Technologies, Carlsbad, CA, USA, cat. No. 15140122), 10 mM HEPES (Thermo Fisher, Fair Lawn, NJ, USA, cat. no. 15-630-080), 100 mg/mL Primocin<sup>®</sup> (InvivoGen, San Diego, CA, USA, cat. no. ANT-PM-1), 1 $\times$  B-27<sup>™</sup> supplement (Gibco, Thermo Fisher, Fair Lawn, NJ, USA, cat. no. 17504-044), 1.25 mM N-acetyl-L-cysteine (Sigma-Aldrich, St. Louis, MO, USA, cat. no. A9165), 10 mM nicotinamide (Sigma-Aldrich, St. Louis, MO, USA, cat. no. N0636), 0.5 mM A83-01 (Tocris, Bristol, UK, cat. no. 2939), 0.5 mg/mL hydrocortisone (Sigma-Aldrich, St. Louis, MO, USA, cat. no. H0888), 10 mM Forskolin (R&D systems, Minneapolis, MN, USA cat. no. 1099), 100 nM  $\beta$ -estradiol (Sigma-Aldrich, St. Louis, MO, USA, cat. no. E2758), 16.3  $\mu$ g/mL bovine pituitary extract (Thermo Fisher, Fair Lawn, NJ, USA, cat. no. 13028014), 10 ng/mL recombinant human FGF-10 (PeproTech, Cranbury, NJ, USA, cat. no. 100-26), 5 ng/mL recombinant human FGF-7 (PeproTech, Cranbury, NJ, USA, cat. no. 100-26), 37.5 ng/mL recombinant human Heregulin Beta-1 (PeproTech, Cranbury, NJ, USA, cat. no. 100-03), 5 ng/mL recombinant human EGF (PeproTech, Cranbury, NJ, USA, cat. no. AF-100-15), 0.5 nM WNT Surrogate-Fc fusion protein (ImmunoPrecise, Victoria, CA, cat. no. N001), 100 ng/mL R-Spondin1 (PeproTech, Cranbury, NJ, USA, cat. No. 120-38), and 1% Noggin-Fc fusion protein conditioned medium (ImmunoPrecise, Victoria, CA, cat. no. N002). Media was changed every 2–3 days and organoids passaged every 7–10 days.



#### 2.4.2. RNA Sequencing of Patient-Derived Organoids

Actively proliferating organoid cultures were dissociated with Gibco™ TrypLE™ Select Enzyme (Thermo Fisher Scientific, Fair Lawn, NJ, USA, cat. No. 12563-011) containing 10 µM Y-27632 ROCK inhibitor (AbMole BioScience, Houston, Texas, USA, cat. No. M1817) and 10 µg/mL DNase I (Sigma-Aldrich, St. Louis, MO, USA, cat. No. DN25) to generate a single-cell suspension. Total RNA was extracted using the Arcturus™ PicoPure™ RNA Isolation Kit (Thermo Fisher Scientific, Fair Lawn, NJ, USA, cat. No. KIT0204) following the manufacturer's protocol. The RNA concentration and purity were evaluated using a NanoDrop™ 8000 Spectrophotometer (Thermo Fisher Scientific, Fair Lawn, NJ, USA). RNA samples were stored at −80 °C and shipped on dry ice to Genewiz (Azenta US, South Plainfield, NJ, USA) for RNA sequencing. The RNA Integrity Number (RIN) ranged from 8.2 to 9.2 across the samples sequenced. Libraries were prepared according to Genewiz's standard RNA-seq protocols. Sequencing was performed on an Illumina® HiSeq® platform (Illumina, San Diego, CA, USA) (configuration HiSeq 2 × 150 PE HO HiSeq 2 × 150 bp). For sequencing analyses, the raw reads underwent quality assessment and trimming using Trimmomatic v0.36 to remove adapter sequences and low-quality bases. The cleaned reads were then aligned to the *Homo sapiens* GRCh38 reference genome (ENSEMBL) using the STAR aligner v2.5.2b, generating alignment files in BAM format. These BAM files served as the basis for quantifying gene expression and performing subsequent differential expression analysis.

#### 2.4.3. Scatter Plot and Heatmap Analyses

Gene expression data were normalized using DESeq2 v1.38.3, which adjusts for library size and variance across samples. To examine the relationship between *ITGB4* and cell cycle activity, the average expression of KEGG-defined cell cycle genes was plotted against the expression of *ITGB4* on a log-log scale. A linear regression model was fitted. The strength of correlation was reported using R-squared and *p*-values.

Heatmaps were created for genes involved in cell cycle and cell-matrix adhesion. Expression values were z-score-normalized across samples for each gene, and genes with no variation or missing values were excluded. Heatmaps were generated using the pheatmap v1.0.12 in R v4.2.2 and hierarchical clustering applied to genes only.

#### 2.4.4. Drug Assays in Patient-Derived Organoids

Grown organoids ranging 30–90 µm in diameter were dissociated with Gibco™ TrypLE™ Select Enzyme (Thermo Fisher Scientific, Fair Lawn, NJ, USA, Cat. No. 12563-011) containing 10 µM Y27632 (AbMole BioScience, Houston, Texas, USA, cat. No. M1817) and 10 µg/mL of DNase I (Sigma-Aldrich, St. Louis, MO, USA, Cat. No. DN25) for 10 min at 37 °C. TrypLE solution was then neutralized with Advanced DMEM/F12 containing 1 × Gibco™ GlutaMAX (Thermo Fisher Scientific, Fair Lawn, NJ, USA, Cat. No. 35050-079), 1 × penicillin-streptomycin (10,000 U/mL) (Life Technologies, Carlsbad, CA, USA, Cat. No. 15140122), 10 mM HEPES (Thermo Fisher Scientific, Fair Lawn, NJ, USA, Cat. No. 15-630-080), 100 µg/mL Primocin® (InvivoGen, San Diego, CA, USA, Cat. No. ant-pm-1), 10 µM Y27632, and 10 µg/mL DNase I. Next, to obtain a single-cell suspension, dissociated organoids were mechanically sheared using a 1 mL syringe with a 30-gauge needle followed by centrifugation at 300 × *g* for 5 min at 4 °C. The cell pellets were then resuspended at 100 cells/µL in ice-cold 70% Cultrex® Reduced Growth Factor BME, Type 2, PathClear™ (Cultrex BME) (R&D Systems, Minneapolis, MN, USA, Cat. No. 3533-010-02) diluted in organoid medium containing 10 µM Y27632 (AbMole BioScience, Houston, Texas, USA, cat. No. M1817) and 10 µg/mL DNase I and kept on ice until use. Inside a tissue culture hood, the single-cell solution was then plated into cell-repellent, clear-bottom 384-well

plates (Greiner Bio-One, Monroe, NC, USA, cat. no. 781976) using an Assist Plus pipetting robot (Integra Biosciences, Hudson, NH, USA, cat. no. 4505) with a Voyager II automatic pipette (Integra, cat. no. 4732). During dispensing, source plates were kept on an integrated active cooling block (Inheco, Planegg, DE, cat. no. 7000190). Using a pre-programmed plating protocol (VIALAB software, v3.1.1), 10  $\mu$ L of cell suspension was dispensed to each assay well for a final density of 1000 cells per well. Assay plates were then placed into an incubator for 10 min at 37 °C to allow the Cultrex BME to polymerize. After 10 min, plates were returned to the tissue culture hood and 20  $\mu$ L of organoid media containing 10  $\mu$ M Y27632 (AbMole BioScience, Houston, Texas, USA, cat. No. M1817) and 10 mg/mL DNase I (Sigma-Aldrich, St. Louis, MO, USA, Cat. No. DN25) were added to each assay well with an Integra pipetting robot, as above.

Prior to drug experiments, the single-cell suspension was plated in two separate plates to determine the seeding variability at plating and organoid density at the time that Cisplatin would be added (day 7 after plating) in subsequent drug experiments. A total of 308 wells were plated, while the remaining wells were filled with media alone to avoid excessive evaporation. Organoids were fed with organoid media without Y27632 or DNase I at day 4 after plating using the Integra pipetting robot as above. CellTiter-Glo 3D Cell Viability Assays (Promega, Madison, WI, USA, cat. no. G9683) were performed following the manufacturer's instructions the next day in one of the plates (20–24 h after plating) for cell density variability at plating, and at day 7 (second plate) for organoid quantification. These results inform the number of organoids at the timepoint that Cisplatin would be added in drug experiments. Luminescence values were quantified using a Clariostar Plus plate reader (BMG Labtech, Ortenberg, DE, cat. no. 0430-501).

For drug experiments, single cells resulting from organoid dissociation were plated as described above. After 4 days, 20  $\mu$ L of organoid media without Y27632 or DNase I was added to each assay well, using the Integra pipetting robot as above. After feeding, 100 nM or 400 nM of Palbociclib (Selleckchem, Houston, Texas, USA, cat. no. S1116) was added to the treatment wells and 0.1% DMSO (Sigma, cat. no. D2650) to the vehicle control wells using an I.DOT S automated liquid handler (Dissipendix, Stuttgart, DE). After 72 h, using the I.DOT liquid handler, Cisplatin (Selleckchem, cat. no. S1166) was added in a 9-point serial dilution, with doses ranging between 22.9 nM and 150  $\mu$ M to both Palbociclib-treated and vehicle control wells. In parallel, additional wells were treated with 10  $\mu$ M Staurosporine (Selleckchem, Cat. No. S1421) as a killing control. Next, the plates were sealed with a semi-porous membrane (Sigma-Aldrich, Cat. No. Z380059) and placed in the incubator at 37 °C undisturbed for 5 days. At the end of drug treatments, cell viability was quantified using CellTiter-Glo 3D Cell Viability Assay (Promega, Madison, WI, USA, cat. no. G9683) and luminescence was quantified using a Clariostar Plus plate reader (BMG Labtech, Ortenberg, DE, cat. no. 0430-501) as described above. As a complementary approach, organoid numbers and size were quantified at the final time point (day 12) using image-based quantification. Bright-field images were taken with a Keyence BZ-X810 microscope (Keyence, Osaka, Japan) and organoids per well (i.e., number of objects), as well as total surface area occupied by all the organoids (i.e., objects) in each well, were quantified with optimized pipelines using the Keyence Hybrid Cell Count Analysis Software (BZ-H4C, Keyence, Osaka, Japan).

#### 2.4.5. Data Analysis and Statistics

IC<sub>50</sub>, R<sup>2</sup>, and AUC values for each drug treatment were calculated with GraphPad Prism v10.0.3. Results are presented as means  $\pm$  SD. The number of independent biological or technical replicates is indicated. The statistical significance was determined by ordinary

one-way ANOVA and Tukey's multiple comparisons test with a single pooled variance, as indicated in each figure.

## 2.5. Bioinformatics Analysis of TCGA Ovarian Cancer Transcriptomic Data

### 2.5.1. Data Retrieval and Preprocessing

RNA sequencing data were downloaded from The Cancer Genome Atlas (TCGA), specifically for the ovarian cancer project (TCGA-OV). These data were accessed using the TCGA biolinks v2.26.3, part of the Bioconductor v3.14, an open-source project that provides tools and packages for the genomic analysis in the R v4.2.2 programming environment [14]. These data included STAR Counts, which is a gene expression quantifications method. The raw data were formatted into an expression matrix using the GDCprepare function. To ensure comparability across samples, the expression data were normalized to Transcripts Per Million (TPM) using the DESeq2 v1.38.3, which adjusts for variations in sequencing depth and gene length [15]. Using the tidyverse v2.0.0, expression data from individual patients were combined into a single dataset. This dataset included TPM values, aligned gene identifiers and patient identifiers, and the combined data were then saved in a TSV format for subsequent analyses.

### 2.5.2. t-SNE Visualization of Transcriptomic Data

Utilizing the Rtsne v0.16 in R, the t-Distributed Stochastic Neighbor Embedding (t-SNE) was performed. This method was applied to visualize patterns of gene expression across ovarian cancer samples. In the t-SNE plot, predefined gene sets associated with GOBP\_CELL\_MATRIX\_ADHESION [16] and KEGG\_CELL\_CYCLE [17] were highlighted with colors, depicting a non-quantitate perspective of transcriptomic data structure and the relationships among these two gene sets.

### 2.5.3. Gene Set Variation Analysis (GSVA) and Correlation Analysis

Gene Set Variation Analysis was executed using the GSVA v1.46.0 in R. This method delivers a non-parametric, unsupervised method to estimate gene set enrichment across the samples [18]. First, the two gene sets, GOBP\_CELL\_MATRIX\_ADHESION" and "KEGG\_CELL\_CYCLE", were extracted from the Molecular Signatures Database (MSigDB) [19,20]. Then, the enrichment scores were derived for each gene set across the samples. Having the GSVA scores, pairwise correlations between gene sets were calculated using Pearson's correlation method. A heatmap was then generated to visually represent these correlations using the ggplot2 v3.4.4. Finally, hierarchical clustering was applied to cluster similar gene sets on the heatmap.

### 2.5.4. Analysis of Cell Cycle Gene Expression by ITGB4 Levels in Ovarian Cancer

To explore the differential expression of cell cycle genes regarding *ITGB4* expression in ovarian cancer, we stratified samples into three groups based on the quantiles of *ITGB4* expression levels. The top 20th percentile was annotated for high expression, the 20th to 80th percentiles for mid expression, and the lowest 20th percentile for low expression. Following the sample classification, a heatmap was generated to visually represent the expression profiles of cell cycle-related genes across the high-, mid-, and low-*ITGB4* expression groups.

### 2.5.5. Gene Ontology (GO) Enrichment Analysis

Subsequently, a Gene Ontology (GO) enrichment analysis was performed to determine the biological processes that were highly upregulated or downregulated in the high *ITGB4* group versus low *ITGB4* group. This analysis used the clusterProfiler v4.6.2 and identified significant GO terms with *p*-values adjusted for multiple testing using the Benjamini--

Hochberg method [21]. Finally, the significant GO terms were visually represented in bar plots using the `enrichGO` function for each of the two categories of upregulated and downregulated gene sets.

#### 2.5.6. Heatmap of RNA-Seq Differential Gene Expression (DEG)

To visually analyze the differential expression of DEGs in Palbociclib-treated spheroids compared to controls, we utilized the `pheatmap` v1.0.12 in R v4.2.2. The gene expression data were first preprocessed to ensure only genes with significant differential expression were included. The expression data were then normalized to minimize variance; this normalization involved scaling each gene's expression levels by subtracting the mean and dividing by the standard deviation of that gene across samples. A heatmap was generated to display the normalized data. Clustering was applied to the rows (genes) to group genes with similar expression patterns.

To focus on specific biological processes across the RNA-seq data, gene sets related to “GOBP\_CELL\_MATRIX\_ADHESION” and “KEGG\_CELL\_CYCLE” were retrieved from the Molecular Signatures Database (MSigDB). The entire gene expression matrix was filtered to include only the selected gene set, after which the heatmap was generated as described above.

The code for the analyses described above is available on GitHub (accessed on 14 April 2025) at [https://github.com/pbabvey/cellProliferation\\_matrixAdhesion](https://github.com/pbabvey/cellProliferation_matrixAdhesion).

### 2.6. RNA-Seq of Palbociclib-Treated Spheroids

#### 2.6.1. Cell Treatment and Spheroid Formation

HEYA8 cells were pre-treated with 500 nM Palbociclib (Selleckchem, Houston, TX, USA, cat. no. S1116) or the carrier control for 72 h. Following treatment, cells were seeded into ultra-low-attachment plates as spheroids in a growth medium containing 2% Matrigel, as previously described in this paper's methodology for 3D spheroids and Matrigel supplementation. Spheroids were allowed to grow for seven days under standard culture conditions.

#### 2.6.2. RNA Extraction and Quality Assessment

Total RNA was extracted from spheroids using the E.Z.N.A.<sup>®</sup> Total RNA Kit (Omega Bio-tek, Norcross, GA, USA) according to the manufacturer's protocol. The concentration and purity of RNA were evaluated using a NanoDrop 2000 spectrophotometer (Thermo Fisher Scientific). The RNA samples were subsequently stored at  $-80^{\circ}\text{C}$  in a freezer before being shipped on dry ice to Genewiz (Azenta US, South Plainfield, NJ, USA) for RNA sequencing.

#### 2.6.3. RNA Sequencing Workflow

The RNA sequencing was sent to GENEWIZ (Azenta Life Sciences, South Plainfield, NJ, USA). The process started with PolyA-based mRNA enrichment. Then mRNA fragmentation and cDNA synthesis were performed through first- and second-strand priming. Subsequent steps included end-repair, 5' phosphorylation, and adenine (dA)-tailing followed by adaptor ligation. The libraries were enriched using PCR. Sequencing was performed on an Illumina HiSeq 2500 device, producing paired-end 150 bp reads. The raw sequencing data underwent quality assessment and trimming to remove adapters and low-quality bases using Trimmomatic v0.36. Next, the cleaned reads were aligned to the *Homo sapiens* GRCh38 reference genome (ENSEMBL), using STAR v2.5.2b. Gene hit counts were obtained using featureCounts from the Subread v1.5.2. The resulting count data were used for subsequent differential expression analyses.

#### 2.6.4. Differential Expression Analysis

Using DESeq2, a comparison of gene expression between Palbociclib-treated and control samples was performed. Statistical significance was determined through the Wald test, which computed  $p$ -values and log<sub>2</sub>-fold changes. Genes with adjusted  $p$ -value (Padj) < 0.05 and an absolute log<sub>2</sub>-fold change > 1 were called as differentially expressed genes (DEGs).

#### 2.6.5. Gene Set Enrichment Analysis

Gene set enrichment analysis (GSEA) was performed using GSEA\_4.2.2 software [22] against selected gene sets from the Molecular Signatures Database (MSigDB 7.5) [19]. The Signal2Noise metric was applied for ranking, and 1000 permutations were used. Results with a false discovery rate (FDR) < 0.25 were considered significant.

#### 2.7. Plasmids and Cloning

First, the pCW57.1 vector (Addgene plasmid, #41393; Addgene, Watertown, MA, USA), which contains a TRE (Tetracycline Response Element) promoter, allows for the inducible expression of genes in the presence of tetracycline or its analog doxycycline. The pCW57.1 vector was modified by inserting a T2A peptide fused to a fluorescent protein marker (mAG monomeric Azami-Green). The T2A-mAG cassette was PCR-amplified from the pBOB-EF1-FastFUCI-Puro plasmid (Addgene plasmid, #12337). Primers were designed to introduce overhangs compatible with NEBuilder HiFi DNA Assembly (New England Biolabs, Ipswich, MA, USA). The PCR product and the pCW57.1 vector were assembled using Gibson Assembly to generate the intermediate vector, Assembled\_pCW\_T2A. The assembled PCR products were then purified from the agarose gel using the Qiagen Gel Extraction (Kit Qiagen, Hilden, Germany). The *ITGB4* coding sequence was PCR-amplified from the pRc/CMV-Beta(4)Integrin (Addgene plasmid, #16265) using a primer pair designed to introduce overhangs complementary to the T2A sequence present in the Assembled\_pCW\_T2A vector. Resulting PCR products and the Assembled\_pCW\_T2A backbone were co-assembled using NEBuilder HiFi DNA Assembly to ultimately yield the construct PCW\_T2AMAG\_ITGB4\_Assembled. This construct included a bicistronic design with mAG, which is a reporter gene downstream of the *ITGB4* sequence, separated by a T2A peptide to allow for their concurrent expression. The expression of green fluorescence in these cells served as an indicator of successful *ITGB4* overexpression.

##### 2.7.1. Plasmid Transformation and Expansion

The constructed plasmid is transformed to competent *E. coli* cells by the method of heat shock for bacterial transformation. Transformation colonies were selected on LB agar plates containing ampicillin. The positive colonies were grown in LB broth and then plasmids isolated with a standard miniprep kit (Qiagen, Hilden, Germany). To check the correctness of the assembled construct, enzymatic digestion and thereafter, electrophoresis, were performed. The resulting fragments were analyzed on an agarose gel to confirm correct assembly based on the size and pattern of the expected fragments.

##### 2.7.2. Lentivirus Production

Lentivirus was prepared by transfection of HEK293T with a mixture of packaging plasmids psPAX2 (Addgene, #12260) and pMD2.G (Addgene, #12259) with the lentiviral vector PCW\_T2A-MAG-ITGB4\_Assembled and incubated in serum-free Opti-MEM (Gibco) and Lipofectamine 3000 (Invitrogen). The medium was refreshed the following day. The viral particles were collected from the supernatant of the cell culture at 48 and 72 h post-transfection. The viral supernatant was then collected and used for the transduction of



target ovarian cancer cell lines, HEYA8 and OV-90. Transduction was performed by adding viral supernatant and polybrene (Santa Cruz Biotechnology, Dallas, TX, USA) to cell culture at a final concentration of 10 µg/mL. Following transduction, the cells were incubated in normal growth conditions for 24 to 48 h before selection pressure was applied by using an appropriate antibiotic. Post-selection, the presence and expression of ITGB4-T2A-MAG fusion protein were confirmed by Western blot analysis, with and without doxycycline (Sigma-Aldrich, #D9891) induction.

### 2.8. Western Blot Analysis

Cells were washed twice with PBS, lysed on ice-cold RIPA buffer (Cell Signaling Technology, Danvers, MA, USA), supplemented with Halt™ Protease Inhibitor Cocktail (Thermo Fisher), then collected using a cell scraper while kept on ice. Cell lysates were pelleted at  $20,000 \times g$  for 20 min, the supernatant was collected, and the protein concentration was determined by BCA assay (Pierce) according to the manufacturer's instructions. The lysates were then combined with 6X sample buffer, boiled at 95 °C for 10 min, followed by loading and resolution by electrophoresis on a polyacrylamide gel. Proteins were then transferred to Immobilon® PVDF transfer membranes (Millipore Sigma, Burlington, MA, USA), which were blocked with 5% non-fat milk in Tris-buffered saline containing 0.1% *v/v* Tween-20 (TBST) for 30 min at room temperature. Afterwards, membranes were incubated with primary antibodies overnight at 4 °C in TBST containing 5% non-fat milk. Membranes were then washed three times with TBST and incubated in an HRP-conjugated secondary antibody (1:10,000) for 1 h at room temperature. Membranes were then washed three times in TBST. Membranes were developed using Immobilon™ Forte enhanced chemiluminescent substrate (Millipore Sigma, Burlington, MA, USA) and visualized using an iBright CL1500 (Thermo Fisher). The following primary antibodies were used in this study: Integrin β4 (LifeSpan BioSciences, Seattle, WA, USA; #LS-C357939), GAPDH (Santa Cruz Biotechnology, #sc-47724). HRP-conjugated secondary antibodies were purchased from Santa Cruz Biotechnology (Dallas, TX, USA).

### Quantification of Western Blot Data

Protein band intensities for integrin β4 were quantified using the Thermo Fisher online tool. Files in G2I format, obtained from iBright, were analyzed to determine the median intensity of each integrin β4 band. These values were then normalized to the corresponding GAPDH intensities to control for loading differences. To facilitate comparison across cell lines, all results were further normalized to HEYA8 cells. Data visualization was performed using the ggplot2 v3.4.4 in R language.

### 2.9. Flow Cytometry

We performed flow cytometry to measure the integrin β4 expression on the cell surface of OC cells. Cells were harvested by trypsinization, collected by centrifugation, and washed twice with PBS containing 2% FBS. An automated cell counter was used to count the cells ( $5 \times 10^5$  to  $1 \times 10^6$ ) and stained with monoclonal integrin β4 antibody (LifeSpan BioSciences, # C357939) at 0.75 µg per  $10^6$  cells and incubated for 1 h at room temperature. Cells were then washed twice with PBS, fixed in 4% paraformaldehyde (PFA) for 15 min and washed again. Cells were incubated with Alexa Fluor 568 secondary antibody (Invitrogen, #A-11011) at a 1:500 dilution and followed by washing and resuspending in PBS. In parallel, cells stained only with the secondary antibody were used as control to determine the background signal. To determine cell viability, adherent cells were trypsinized, centrifuged at  $300 \times g$  for 5 min, and washed twice with PBS containing 2% FBS. Cells were then incubated on ice with PBS containing 2% FBS and 2 µg/mL propidium iodide (PI) (Molecular Probes, Eugene, OR, USA). Data acquisition was performed using an Attune NxT Flow Cytometer

(Thermo Fisher) and analyzed with FlowJo v10.10.0 (FlowJo, Ashland, CA, USA). The cell death was reported as the percentage of PI-positive cells and cell viability was reported as the percentage of PI-negative cells.

### 2.10. Statistical Analysis

Statistical analyses were performed using GraphPad Prism v9.5.1 (GraphPad Software, San Diego, CA, USA) and statistical significance was determined with unpaired, two-tailed, parametric t-tests and adjustment for multiple comparisons (Benjamini–Hochberg method), one-way ANOVA followed by Tukey’s multiple comparisons test, or a two-way ANOVA. In all the statistical analysis,  $p \leq 0.05$  was considered statistically significant.

## 3. Results

### 3.1. Examinations of Ovarian Cancer TCGA Datasets Reveal an Inverse Correlation Between Cell-Matrix Adhesion and Cell Cycle Gene Expression

To determine the relationship between cell cycle regulation and cell-extracellular matrix (ECM) adhesion in OC, we analyzed 433 TCGA ovarian cancer transcriptomes downloaded from the Genomic Data Commons (GDC) Data Portal through custom R scripts. These transcriptomes represent the most prevalent subtype of ovarian cancer, ovarian serous cystadenocarcinoma, which primarily includes high-grade serous ovarian carcinoma [23]. We employed the t-distributed Stochastic Neighbor Embedding (t-SNE) method to visualize the expression landscape of genes involved in both the cell cycle and cell-matrix adhesion pathways. This dimensionality reduction technique helped us reveal clusters that represent distinct expression patterns of these gene groups across the patient cohort. By overlaying specific gene markers from the Molecular Signature Database (MSigDB; <https://www.gsea-msigdb.org/gsea/msigdb/>, accessed on 20 February 2023), specifically, the gene sets GOBP\_CELL\_MATRIX\_ADHESION and KEGG\_CELL\_CYCLE on the t-SNE plot, we observed clear clustering patterns, indicating the potential relationship between these gene sets (Figure 1A). To further elucidate the relationship between the cell cycle and cell-matrix adhesion genes, we conducted a correlation analysis, calculating the pairwise correlations between these two sets of genes. Using the Gene Set Variation Analysis (GSVA), we identified a negative correlation between the expression of cell-matrix adhesion genes and many of the genes regulating cell cycle progression (Figure 1B). Notably, our pairwise analysis demonstrated a negative correlation between cell cycle genes and laminin-binding integrin  $\beta 4$  (Figure 1B arrow). Interestingly, our previously published experiments provided evidence that increasing deposition of laminin-rich ECM suppresses cell proliferation [2]. These results suggest the possibility that *ITGB4* expression levels vary depending on the cell cycle status in ovarian cancer cells. In addition to the predominant negative correlation with *ITGB4*, several genes positively correlated with cell cycle regulators (red portion in Figure 1B). Some of these genes, such as *PTPRC* (*CD45*), *LILRB1*, and *IKZF1*, are involved in immune response, suggesting a potential role in immune signaling in cell proliferation [24,25]. Genes such as *FAP* and *INHBA* are linked to ECM remodeling and fibrosis, which may support proliferation [26]. These findings highlight the interplay between immune signaling, the microenvironment, and cell cycle progression.

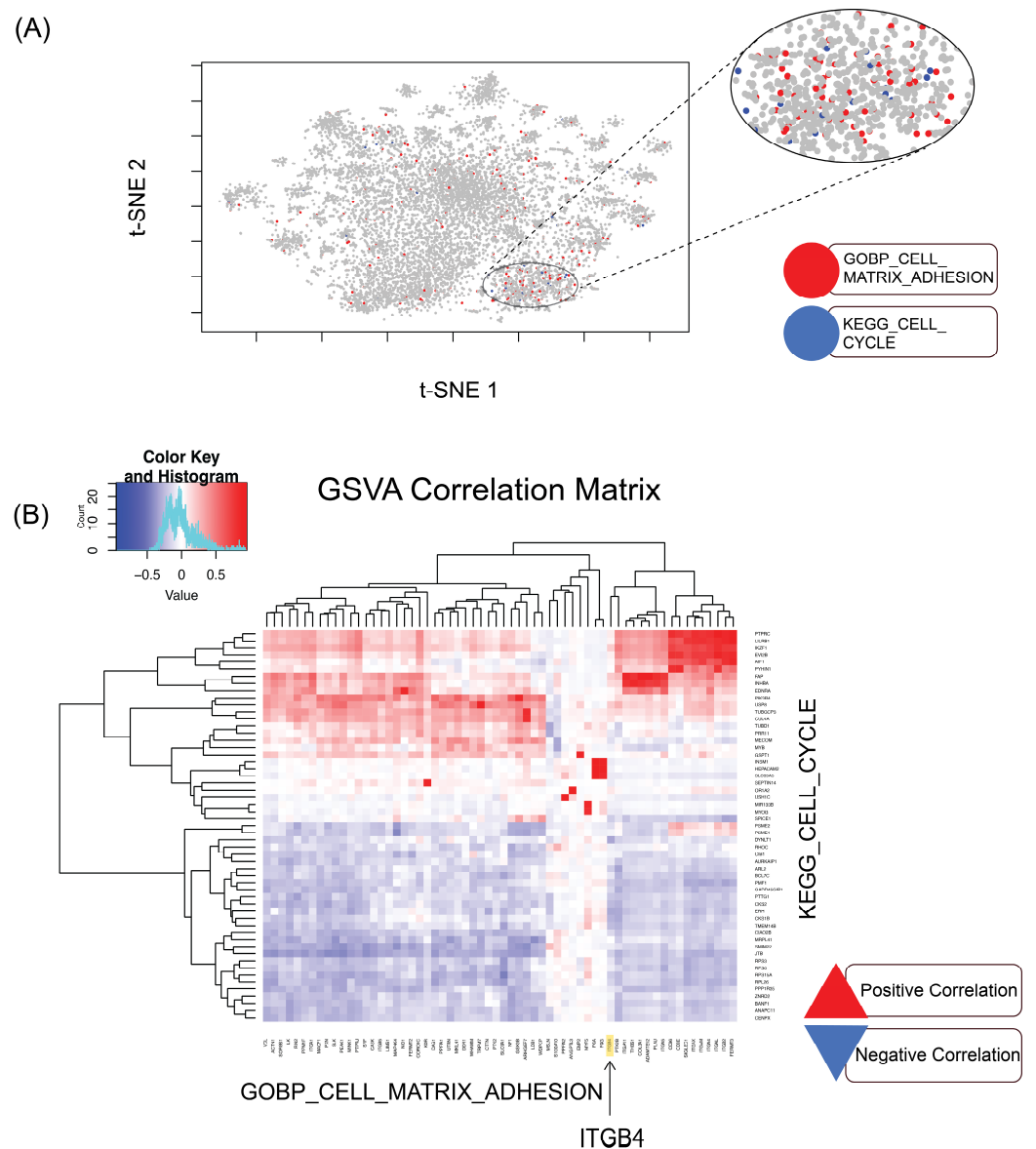


**Figure 1.** Inverse correlation between cell-matrix adhesion and cell cycle gene expression in high-grade serous ovarian carcinoma. **(A)** t-SNE visualization of variance-expressed genes across 433 patient transcriptomes from TCGA-OV. The magnified oval highlights colocalization of cell-matrix adhesion and cell cycle genes, suggesting their connection. **(B)** Correlation analysis between cell cycle and cell-matrix adhesion genes using Gene Set Variation Analysis (GSVA). This analysis demonstrates a significant negative correlation between cell cycle genes and cell-ECM adhesion molecules, including *ITGB4* (arrow).

### 3.2. *ITGB4* mRNA Expression Changes with Cell Cycle Genes in Ovarian Cancer Patients

To test the possibility of whether *ITGB4* mRNA expression levels change in relation to the ovarian cancer cell cycle, we analyzed gene expression profiles across The TCGA ovarian cancer datasets. Patients were categorized based on their *ITGB4* mRNA expression into high, medium, and low groups. Our heatmap analysis (Figure 2A) reveals a striking inverse correlation, where high *ITGB4* expression is associated with the downregulation of some cell cycle genes, suggesting a potential suppressive role of *ITGB4* on cell cycle progression. Conversely, lower *ITGB4* expression levels are linked with upregulated cell cycle gene expression, indicating a more active cell cycle.

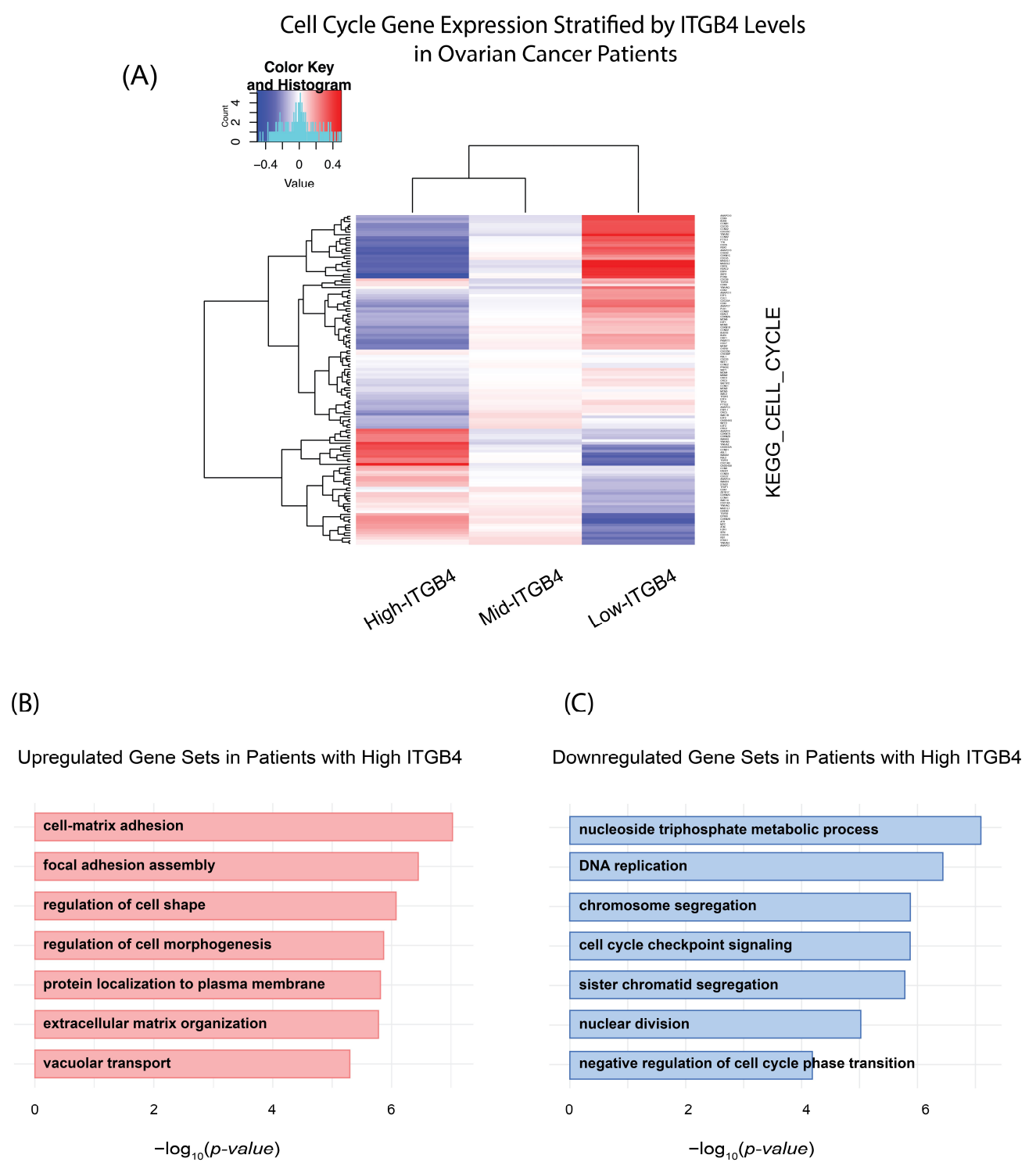


**Figure 2.** Differential expression and functional impact of *ITGB4* in ovarian cancer. **(A)** Heatmap of cell cycle gene expression across ovarian cancer patients, categorized by *ITGB4* mRNA levels. High *ITGB4* (top 20 percentiles) is associated with generally lower expression of cell cycle genes (KEGG\_CELL\_CYCLE), whereas low *ITGB4* (bottom 20 percentiles) is linked to broadly higher expression of these genes. **(B)** Upregulated gene sets in patients with high *ITGB4*. Statistical analysis via t-tests and adjustment for multiple comparisons (Benjamini–Hochberg method) identified cellular processes such as cell-matrix adhesion and extracellular matrix organization that are significantly upregulated. **(C)** Downregulated gene sets in patients with high *ITGB4*. Similar statistical methods reveal significant downregulation in processes related to cell cycle progression and DNA replication, indicating a potential shift towards a more quiescent cellular state.

Furthermore, our gene ontology analysis of ovarian tumor samples with high *ITGB4* expression highlighted several critical cellular mechanisms being influenced. Specifically, we observed a pronounced activation of gene sets associated with cell-matrix adhesion and extracellular matrix organization, suggesting a pivotal role for integrin  $\beta 4$  in modulating the interaction between ovarian cancer cells and their microenvironment (Figure 2B). Conversely, the analysis also revealed a significant downregulation in gene sets related to core cell cycle processes, such as DNA replication, chromosome segregation, and cell cycle checkpoint signaling (Figure 2C). This pattern suggests that high *ITGB4* levels may contribute to a reduction in cell proliferation rates, possibly through inducing a more quiescent cellular state. These findings raised the question of whether high integrin  $\beta 4$  protein expression is inversely correlated with OC cell proliferation.

### 3.3. Integrin $\beta 4$ Protein Expression Inversely Correlates with OC Cell Proliferation

To determine whether integrin  $\beta 4$  protein expression inversely correlates with cell proliferation, we probed integrin  $\beta 4$  protein expression, and measured cell proliferation rates among various OC cell lines, including OVCAR4, OV-90, KURAMOCHI, CAO3, TYK-nu, RMUGS, HEYA8, OVSAHO, and OVCAR3. Western blot analysis revealed the following integrin  $\beta 4$  expression levels in ovarian cancer cell lines: lowest in HEYA8, highest in RMUGS and CAO3, and intermediate in OVCAR4, OV-90, KURAMOCHI, OVSAHO, OVCAR3, and TYK-nu (Figure 3A). Our observations also revealed an inverse relationship between integrin  $\beta 4$  expression and cell proliferation: cells with lower integrin  $\beta 4$  levels (HEYA8) exhibited the highest proliferation rates, while those with higher levels (RMUGS) showed the least (Figure 3C). Three independent experiments were conducted to confirm these results, with the quantification of integrin  $\beta 4$  protein expression (Figure 3B). These findings support the hypothesis that integrin  $\beta 4$  expression is associated with the regulation of cell proliferation.

### 3.4. Inhibition of OC Cell Proliferation with Palbociclib Activates Cell-ECM Adhesion Programs, Expression of Integrin $\beta 4$ and Induces Protection from Cisplatin

So far, our data provide evidence that laminin receptor integrin  $\beta 4$  expression correlates with low OC cell proliferation. Next, we wanted to explore the possibility of whether directly inhibiting cell cycle progression, in cells expressing low levels of integrin  $\beta 4$ , stimulates ECM adhesion programs and integrin  $\beta 4$  expression. To examine this possibility, we treated HEYA8 (integrin  $\beta 4^{\text{low}}$ ) with Palbociclib (Ibrance), an FDA-approved cyclin-dependent kinase 4/6 (CDK4/6) inhibitor. We also observed that in three-dimensional ECM-supplemented HEYA8 cultures, Palbociclib significantly decreased the formation of HEYA8 outgrowths, which are multicellular extensions protruding from spheroids (Figure 4A). Taken together, these data indicate that Palbociclib-treated HEYA8 cells downregulate cell cycle progression programs and inhibit outgrowth formation [2]. Next, we wanted to know whether inhibition of cell proliferation with Palbociclib promotes the expression of cell matrix-adhesion genes. To do this, we performed RNA-sequencing of suspended HEYA8 cell cultures reconstituted with 2% Matrigel and treated with vehicle control or 500 nM Palbociclib (Figure 4A). RNA sequencing revealed that over 2600 genes were differentially expressed (DEGs) in Palbociclib-treated HEYA8 spheroids compared to controls, which highlights the broad impact of Palbociclib on gene regulation (Figure 4B). As expected, Palbociclib treatment significantly downregulated the expression of genes associated with cell cycle progression (Figure 4C). Interestingly, we observed that Palbociclib induced the expression of cell-matrix adhesion and cell-matrix receptor genes, including integrin  $\beta 4$  (Figure 4D).



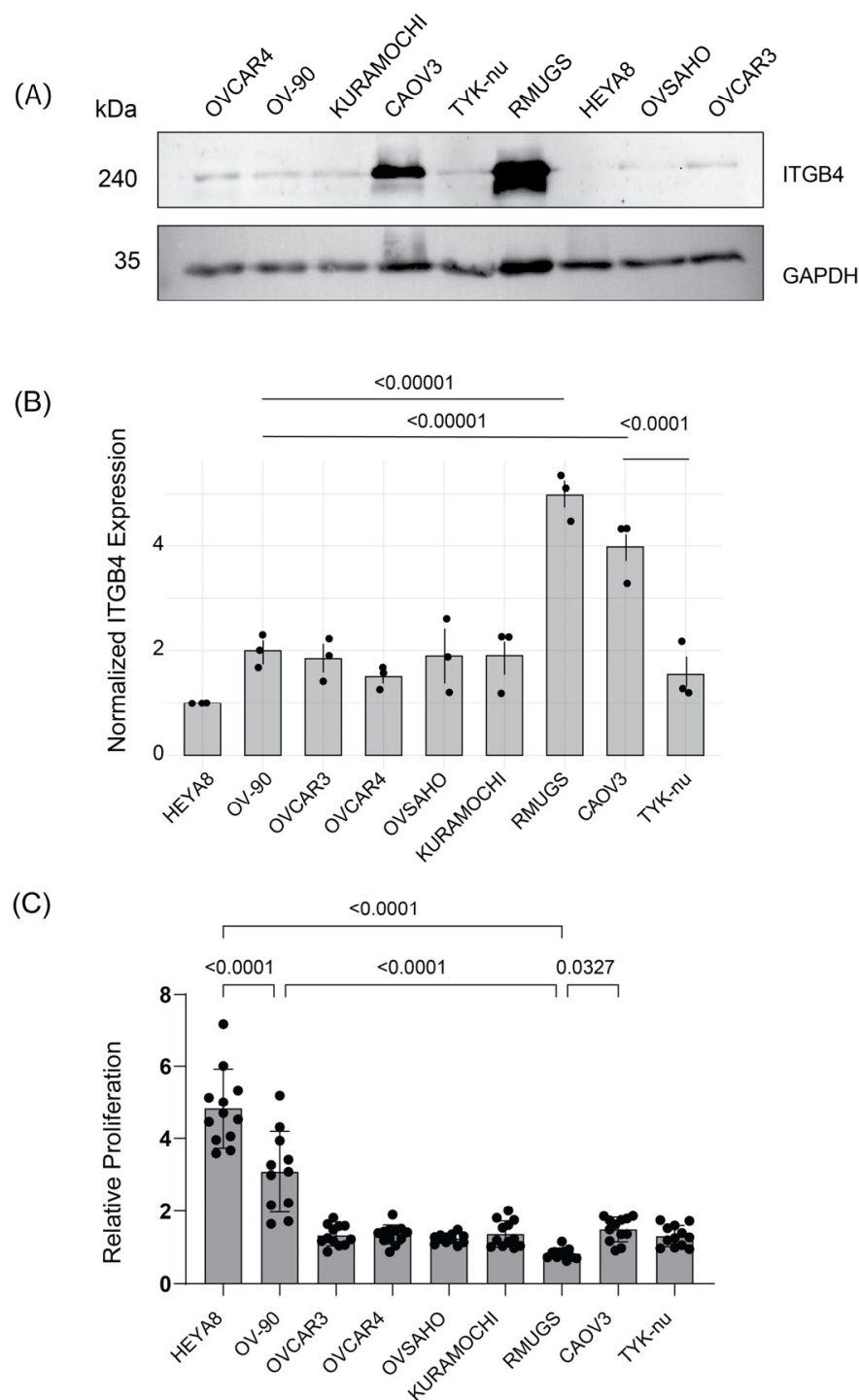


**Figure 3.** Reverse correlation between integrin  $\beta 4$  protein expression and cell proliferation in ovarian cancer cell lines. **(A)** Western blot analysis of integrin  $\beta 4$  and GAPDH protein expression in various OC cell lines. The analysis reveals varying integrin  $\beta 4$  expression levels, with the lowest in HEYA8 and the highest in RMUGS and CAOV3. **(B)** Quantification of normalized integrin  $\beta 4$  expression across the cell lines, derived from three independent experiments (Western blot), showing distinct patterns of integrin  $\beta 4$  expression. Statistical analysis was performed using one-way ANOVA followed by Tukey's multiple comparisons test, indicating significant differences among some of the cell lines ( $p < 0.0001$  for highlighted comparisons). Each dot represents an independent experimental replicate. **(C)** Proliferation rates measured by normalized alamarBlue fluorescence across all nine cell lines, with statistical analysis performed using one-way ANOVA followed by Tukey's multiple comparisons test. These data indicate significant differences in proliferation rates between cell lines with the highest and lowest expression of integrin  $\beta 4$  ( $p < 0.0001$ ). The uncropped blots are shown in Figure S3A,B.

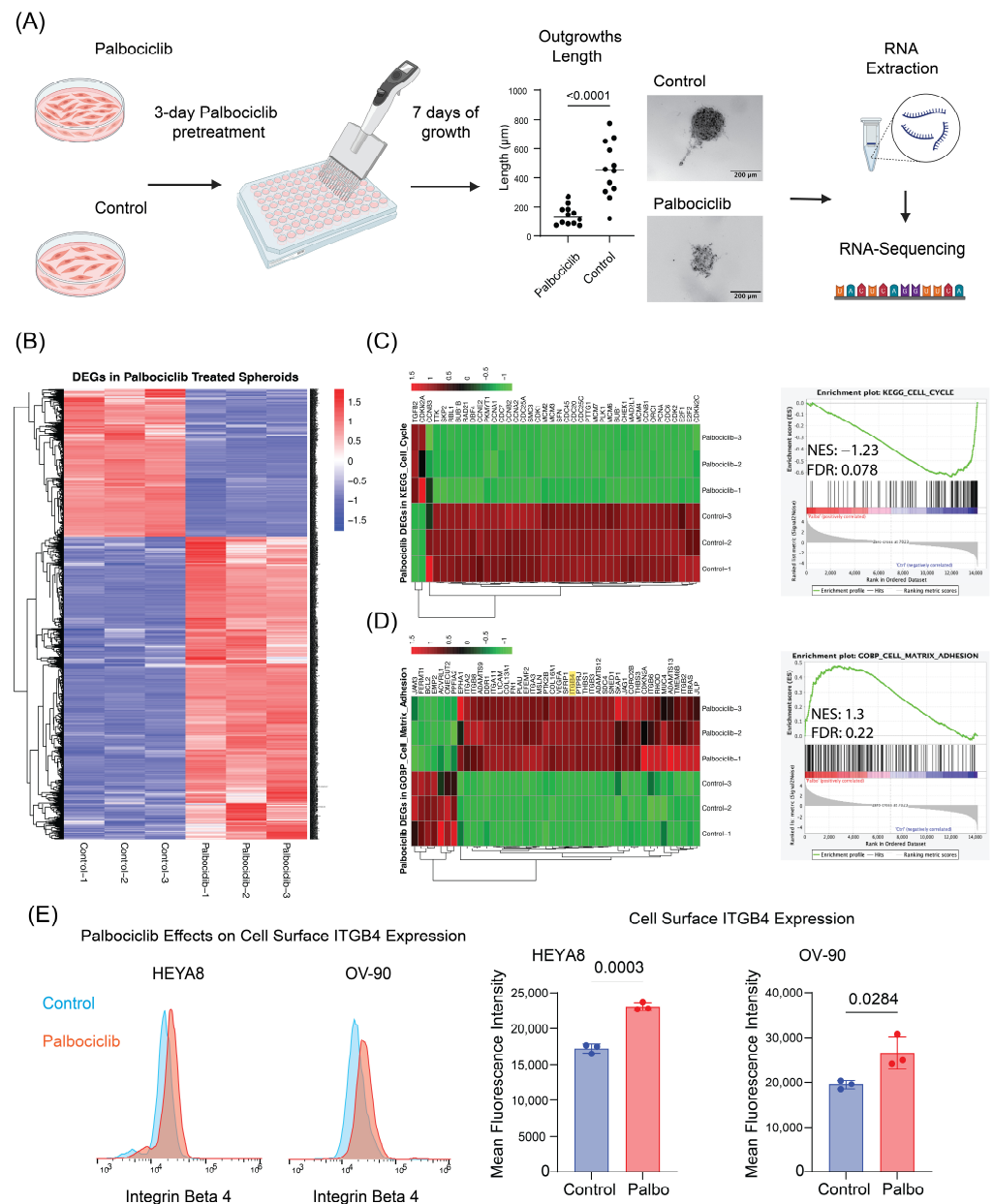


**Figure 4.** Palbociclib effects on *ITGB4* expression and cell cycle genes in ovarian cancer 3D models. **(A)** Schematic of the experimental workflow where HEYA8 cells underwent pretreatment with 500 nM Palbociclib for 3 days, followed by 7 days of growth in 3D spheroid culture. The plot quantifies outgrowth length from the main spheroid in control versus Palbociclib-treated groups. Each point represents one spheroid, analyzed using an unpaired *t*-test. Representative images display spheroid formation in both treated and control groups, with subsequent steps including RNA extraction and sequencing. Arrows represent the experimental sequence. **(B)** Heatmap of differentially expressed genes (DEGs) comparing Palbociclib-treated spheroids to controls, highlighting over 2600 DEGs. In the heatmap, red indicates upregulated and blue indicates downregulated DEGs. **(C)** Heatmap and GSEA plot demonstrating downregulation of cell cycle-related genes (KEGG\_CELL\_CYCLE pathway) in treated spheroids with an NES of  $-1.23$  and an FDR of  $0.078$ . In panels C and D, red indicates upregulation and green downregulation. **(D)** Heatmap and GSEA plot for the GOBP\_CELL\_MATRIX\_ADHESION pathway showing an NES of  $1.3$  and an FDR of  $0.224$ , illustrating differential expression patterns. **(E)** Flow cytometry and quantification of integrin  $\beta 4$  expression changes in HEYA8 and OV-90 cell lines post-Palbociclib treatment. Histograms show the differential cell surface integrin  $\beta 4$  levels, and bar charts quantify the changes in mean fluorescence intensity, with each dot representing an independent biological replicate. Statistical analysis was performed using an unpaired *t*-test, with *p*-values indicated on the charts.

Gene set enrichment analysis (GSEA) was performed based on RNA sequencing data to further investigate the effects of Palbociclib on gene expression in ovarian cancer cells, which supports the illustrated heatmaps quantitatively. Especially, in (Figure 4C—right), the GSEA plot versus KEGG\_CELL\_CYCLE pathway showed that cell cycle-related genes were significantly downregulated when treated with Palbociclib, documented with a normalized enrichment scores (NES) of  $-1.23$  and a false discovery rate (FDR)  $q$ -value of  $0.078$ . GOBP\_CELL\_MATRIX\_ADHESION pathway analysis further provides an NES of  $1.3$  (Figure 4D—right), pointing toward the upregulation of genes involved in cell-ECM adhesion, with an FDR  $q$ -value of  $0.224$ . These data highlight that Palbociclib treatment affects not only gene expression involved in the cell cycle but also significantly affects the gene expression involved in cell-matrix adhesion. We validated Palbociclib-regulation of integrin  $\beta 4$  expression in HEYA8 and OV-90 cells using flow-cytometry-based quantification of cell surface protein expression (Figure 4E).

Next, we wanted to determine whether Palbociclib-mediated suppression of cell proliferation and activation of cell-matrix adhesion programs is associated with reduced response to Cisplatin. To do this, we used a combination of flow cytometry and propidium iodide incorporation assay as a proxy for measuring cell death. In HEYA8 cells, which are characterized by low integrin  $\beta 4$  expression, Palbociclib significantly reduced the percentage of dead cells upon Cisplatin treatment compared to the Cisplatin treatment alone ( $p < 0.0001$ ) (Figure 5A). A similar trend was observed in OV-90 cells, where Palbociclib also significantly reduced Cisplatin-induced cell death ( $p = 0.0116$ ) (Figure 5B). The decrease in Cisplatin sensitivity was less marked in OV-90 cells, possibly because these cells express mid-level of integrin  $\beta 4$  and therefore benefit less from integrin  $\beta 4$  upregulation compared to HEYA8 following Palbociclib pretreatment. The increased integrin  $\beta 4$  expression potentially provides a protective effect, enhancing the resistance to Cisplatin-induced cell death. Furthermore, Gene Set Enrichment Analysis (GSEA) of RNA sequencing data from Palbociclib-treated spheroids demonstrated significant enrichment of Cisplatin resistance gene sets across three independent studies (Kang [27], Tsunoda [28], and Whiteside [29]). The normalized enrichment scores (NES) for these studies were  $1.35$ ,  $1.43$ , and  $1.36$ , respectively, reinforcing the hypothesis that Palbociclib-induced growth arrest enhances Cisplatin resistance (Figure 5C).

These findings suggest that Palbociclib enhances Cisplatin resistance in ovarian cancer cells, with a particularly pronounced effect in low integrin  $\beta 4$ -expressing cells, such as HEYA8, where the upregulation of integrin  $\beta 4$  may play a critical role in reducing Cisplatin sensitivity.

### *3.5. Palbociclib Treatment Modulates Cisplatin Sensitivity in Patient-Derived Ovarian Cancer Organoids*

We next sought to determine whether Palbociclib similarly induce a protective effect to Cisplatin treatment in patient-derived ovarian cancer organoids (PDOs). Thus, we performed drug dose-response assays to Cisplatin, comparing Palbociclib pre-treated vs. untreated PDOs. As expected, Cisplatin treatment induced visible morphological changes in comparison to vehicle controls indicative of PDO sensitivity to Cisplatin. Notably, these morphological changes were of lesser extent in Palbociclib pre-treated conditions (Figure 6A). To quantify responses to these treatments, we measured ATP levels as a surrogate of cell viability at the assay end-point using CellTiter-Glo<sup>®</sup> reagent, revealing a robust, dose-dependent decrease in sensitivity to Cisplatin in Palbociclib-treated PDOs (Figure 6B). We also used an image-based quantification approach at the end-point using the Keyence Cell Count Hybrid Analysis software (BZ-H4C, Keyence, Osaka, Japan) and confirmed that pre-treatment with Palbociclib protects organoids from the Cisplatin-induced cytotoxic effects (Figure S1A,B). These results suggest that the Palbociclib-induced resistance to

Cisplatin can be recapitulated in ovarian cancer patient primary material grown in the form of organoids. The inverse correlation between *ITGB4* expression and cell cycle gene expression was also observed in PDOs, as shown in Figure S2.

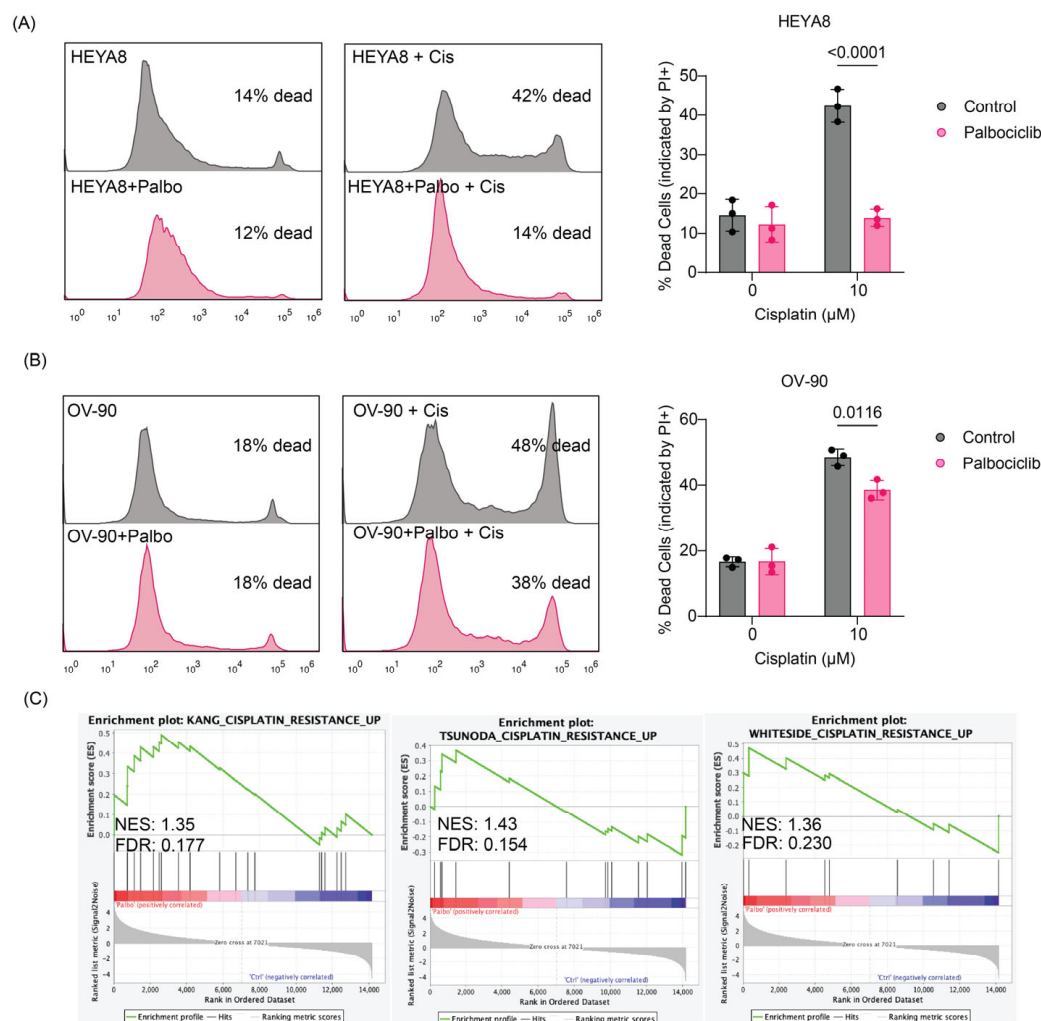


**Figure 5.** Palbociclib-induced Cisplatin resistance in ovarian cancer cells. **(A)** Flow cytometry of HEYA8 cells shows reduced cell death when pretreated with Palbociclib (500 nM) before Cisplatin (10  $\mu$ M) treatment. Histograms show cell death percentages, with bar graphs quantifying the effects across treatments. Each dot represents an independent replicate. Statistical significance from decreased PI+ staining is shown ( $p < 0.0001$ ), analyzed by two-way ANOVA, highlighting interaction effects. **(B)** In OV-90 cells, similar pretreatment reduces Cisplatin-induced cell death, with significant differences ( $p = 0.0116$ ). Each bar graph dot represents a replicate, analyzed via two-way ANOVA. **(C)** GSEA of Palbociclib-treated HEYA8 spheroids shows upregulation of Cisplatin resistance gene sets. NES and FDR for each study are Kang (NES: 1.35, FDR: 0.177), Tsunoda (NES: 1.43, FDR: 0.154), and Whiteside (NES: 1.36, FDR: 0.230), suggesting a link between Palbociclib pretreatment and altered drug response.

### 3.6. Overexpression of Integrin $\beta 4$ Modulates Chemotherapy Response and Reduces Proliferation in Ovarian Cancer Cells

To determine whether integrin  $\beta 4$  expression modulates Cisplatin sensitivity, we utilized a doxycycline-inducible lentiviral system to overexpress integrin  $\beta 4$  protein molecules in both HEYA8 and OV-90 cells. As shown in Figure 7A, we were able to overexpress *ITGB4* in a doxycycline-dependent manner. Forced overexpression of *ITGB4* significantly suppressed proliferation in both integrin  $\beta 4$ -low HEYA8 and integrin  $\beta 4$ -intermediate OV-90 cells ( $p$ -value  $< 0.0001$  and  $= 0.0008$ , respectively), albeit to a lesser extent in OV-

90 cells. These results suggest that the underlying basal levels of integrin  $\beta 4$  expression may modulate cell proliferation rates (Figure 7B). We next measured the impact of integrin  $\beta 4$  overexpression on sensitivity to Cisplatin using propidium iodide incorporation and flow cytometry. In both cell lines, integrin  $\beta 4$  overexpression exhibited significantly reduced Cisplatin-induced cell death compared to controls (Figure 7C,D). Hence, integrin  $\beta 4$  overexpression reduced drug sensitivity. Notably, these effects were to a greater extent in HEYA8, the OC cell line with the lowest integrin  $\beta 4$  levels, suggesting that the acquired expression of integrin  $\beta 4$  in low-expressing cells could have a significant impact in Cisplatin resistance. These findings support the model whereby integrin  $\beta 4$  expression modulates ovarian cancer proliferation and response to chemotherapy (Figure 8).

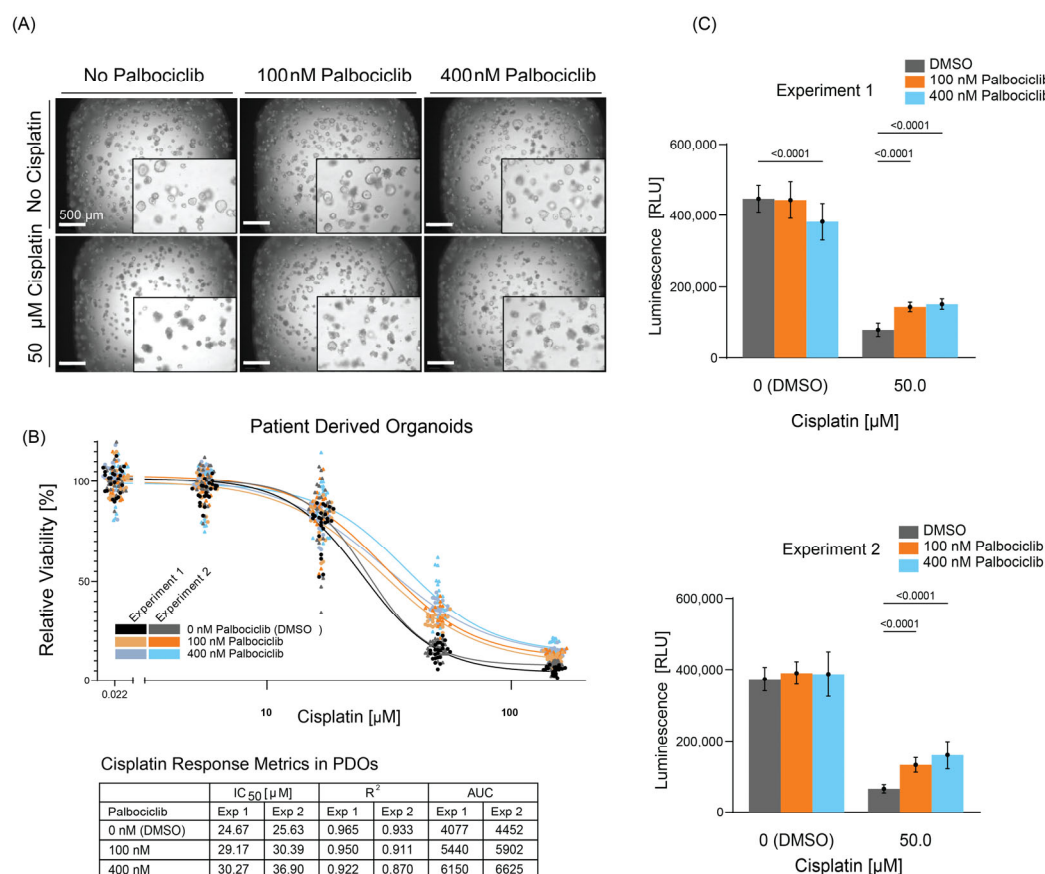


**Figure 6.** Palbociclib treatment decreases sensitivity to Cisplatin in patient-derived organoids (PDO). (A) Representative brightfield images at day 12 show control versus treated PDOs under different concentrations of Palbociclib and Cisplatin. Insets highlight morphological changes. Scale bars: 500  $\mu\text{m}$ . (B) Drug dose–response curves of PDOs for Cisplatin in untreated vs. palbociclib pre-treated PDOs at 100 nM and 400 nM concentrations. Each dot corresponds to one technical replicate (at least 9 replicates per dose in each independent experiment). Table shows  $\text{IC}_{50}$ ,  $R^2$ , and AUC values for 50  $\mu\text{M}$  Cisplatin doses in two independent experiments. (C) Corresponding ATP levels (Relative Light Units, RLU) in PDOs treated with 50  $\mu\text{M}$  Cisplatin after exposure to 100 nM or 400 nM Palbociclib. Levels were normalized to vehicle and Staurosporine-treated control (DMSO). Error bars represent mean  $\pm$  SD of technical replicates. Statistical analysis utilized ordinary one-way ANOVA.



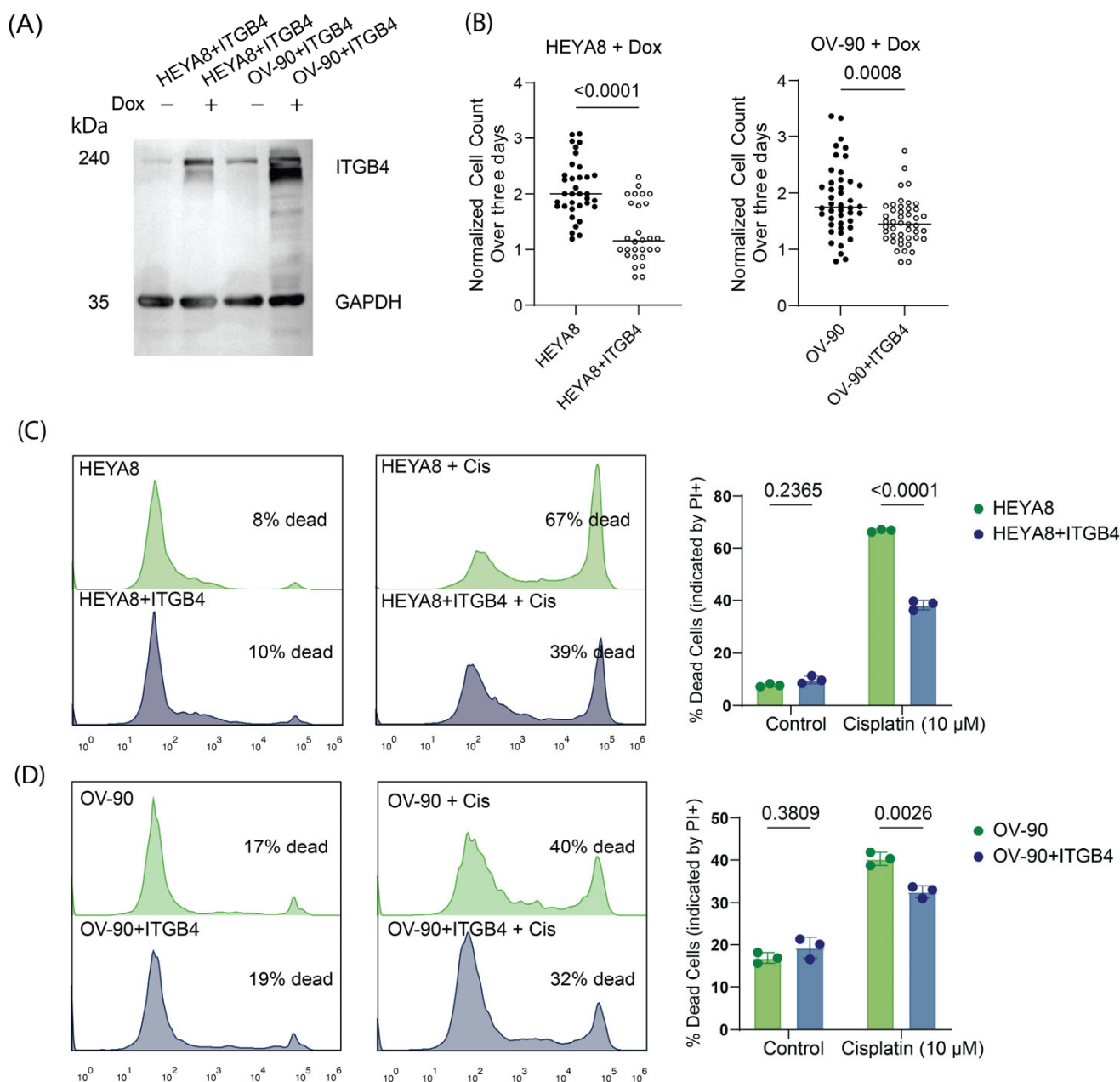


**Figure 7.** Integrin  $\beta 4$  modulates chemotherapy response and reduces proliferation in ovarian cancer cells. **(A)** Western blot analysis demonstrating induced overexpression of integrin  $\beta 4$  in HEYA8 and OV-90 cells treated with doxycycline-inducible *ITGB4* expression systems (doxITGB4). **(B)** Normalized cell count data showing significant suppression of proliferation due to induced overexpression of *ITGB4* in HEYA8 and OV-90 cells. Statistical significance determined by unpaired *t*-tests ( $p < 0.0001$  for HEYA8,  $p = 0.0008$  for OV-90). **(C)** Flow cytometry analysis and bar graphs for HEYA8 cells show that *ITGB4* overexpression reduces Cisplatin-induced cell death, with fewer dead cells in *ITGB4*-overexpressing cells compared to controls under Cisplatin treatment ( $p < 0.0001$ ). Statistical analysis performed using two-way ANOVA test. **(D)** Similar analysis for OV-90 cells, where *ITGB4* overexpression confers increased resistance to Cisplatin. The comparison of native and *ITGB4*-overexpressing cells indicates a decrease in Cisplatin-induced cell death in *ITGB4*-overexpressing cells ( $p = 0.0026$ ), with analysis supported by two-way ANOVA test and  $p$ -values indicated on the chart. The uncropped blots are shown in Figure S3C.

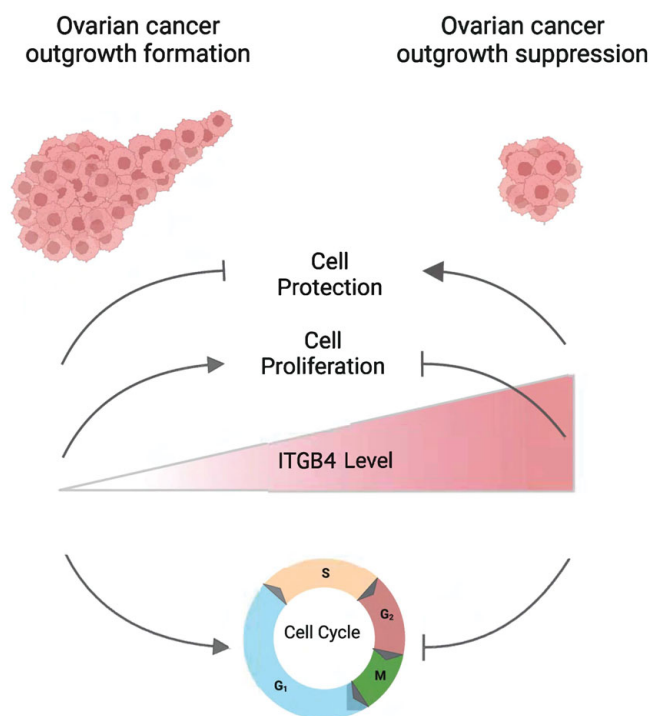


**Figure 8.** Influence of integrin  $\beta 4$  on cell cycle dynamics and cytotoxic drug resistance in ovarian cancer models. This schematic illustrates the correlation between elevated integrin  $\beta 4$  expression and slowdown of cell cycle progression in various ovarian cancer models. Specifically, higher levels of integrin  $\beta 4$  are linked to reduced cellular proliferation, resulting in less outgrowth formation in 3D spheroid models and an increase in resistance to cytotoxic agents such as Cisplatin.

#### 4. Discussion

Our studies provide evidence that growth suppression of cultured OC cells decreases Cisplatin sensitivity and induces integrin  $\beta 4$  expression. Furthermore, we demonstrated that forced expression of *ITGB4* decreased proliferation and Cisplatin sensitivity. Using patient data that are available through TCGA, we have demonstrated an inverse correlation between cell-matrix adhesion and cell-cycle progression. More specifically, we identified that patients' tumors expressing high levels of *ITGB4* mRNA were the less proliferative, raising the question of whether regulation of *ITGB4* expression is linked to cell proliferation. We provide experimental evidence that doxycycline-mediated regulation of *ITGB4* expression can impact OC cell proliferation and their response to Cisplatin, one of the most used chemotherapeutic agents in OC treatment.

Our in vitro experiments on OC cell lines were aligned with our analysis of patients' data from TCGA; OC cell lines with higher integrin  $\beta 4$  protein levels displayed reduced proliferation rates, while those with lower expression proliferated more rapidly. However, it is important to note that some studies on other carcinomas have reported that higher expression levels of integrin  $\alpha 6 \beta 4$  correlate with a greater proliferating fraction, suggesting context-dependent roles of integrin  $\beta 4$  [30], which could be related to the unique matrix compositions observed in different tumor contexts.

The relationship between the growth rate of OC cells and cell-matrix adhesion was further elucidated by RNA-seq data of Palbociclib-treated OC spheroids. Treatment of OC cells with Palbociclib, a known inducer of G<sub>1</sub> cell cycle arrest as a CDK4/6 inhibitor, resulted in the downregulation of cell cycle genes and an upregulation of genes involved in cell-matrix adhesion, interestingly including *ITGB4* as one of the highly upregulated genes. Upregulation of integrin  $\beta 4$  was confirmed by flow cytometry of Palbociclib-treated HEYA8 and OV-90 cells.

Palbociclib-treated cells had reduced sensitivity to the chemotherapeutic agent Cisplatin. Pretreatment with Palbociclib profoundly diminished Cisplatin-induced cell death in HEYA8 cells, which express low-levels of integrin  $\beta 4$ , and less so in OV-90 cells that express an intermediate level of integrin  $\beta 4$ . These data support the idea that baseline integrin  $\beta 4$  expression modulates chemoresistance, particularly in cells that have undergone cell cycle arrest following Palbociclib pretreatment.

The efficacy of Palbociclib is closely associated with the functional status of the Rb protein because CDK4/6 inhibitors mediate the Rb pathway to exert a cell cycle arrest effect. Mutations or loss of Rb predispose cells to resistance against CDK4/6 inhibitors [31]. Indeed, previous studies have shown that cancer cell lines lacking Rb expression fail to respond to Palbociclib treatment [32–34]. HEYA8 and OV-90 cells reportedly express functional Rb protein and thus should be sensitive to the inhibitory action of CDK4/6 [35–37]. It is thus plausible that, following Palbociclib-mediated cell cycle arrest, the upregulation of *ITGB4* can trigger survival signals which diminish the sensitivity of the cells to Cisplatin cytotoxicity. These findings are consistent with reports that integrin  $\beta 4$  promotes cell survival and resistance to apoptotic-inducing agents [7,8].

While our experiments focused on Cisplatin, there is evidence that Palbociclib-induced  $G_1$  arrest can reduce the effectiveness of other DNA-damaging drugs by halting cell cycle progression [33,34]. Integrin  $\beta 4$  has also been linked to resistance against various chemotherapies, including anthracyclines, in breast cancer models [8]. Furthermore, Zhang et al. showed that blocking CDK4/6-dependent Rb phosphorylation activates the mTORC2–Akt pathway, suggesting an alternative survival mechanism under cytotoxic stress [38]. These observations suggest that Palbociclib, combined with elevated integrin  $\beta 4$ , may weaken responses to additional treatments beyond Cisplatin.

The interaction between upregulated integrin  $\beta 4$  and laminin in the ECM activate signaling pathways that promote cell survival and inhibit apoptosis [5,6]. The  $\alpha 6\beta 4$  heterodimer interacts with laminin and can activate signaling cascades such as the PI3K/Akt and NF- $\kappa$ B pathways [39,40]. These pathways are associated with cell survival, invasion, and chemotherapy resistance. Based on this, we hypothesize that the cell cycle is inversely correlated with cell-ECM adhesion, including integrin  $\beta 4$ , and the higher expression of this adhesion molecule suppresses sensitivity to Cisplatin. These findings also suggest that cell cycle inhibition can induce a phenotypic shift towards a more quiescent phenotype, with increased cell adhesion mediated by integrin  $\beta 4$  [41]. These cells are more resistant to treatments that target rapidly dividing cells [42]. We propose a model in which elevated integrin  $\beta 4$  expression slows cell cycle progression and reduces proliferation, thereby increasing resistance to cytotoxic agents like Cisplatin (Figure 8).

In our in vitro study with OC cell lines, high levels of integrin  $\beta 4$  protein were associated with lower proliferation and increased Cisplatin resistance. Additionally, integrin  $\beta 4$  has been shown to protect breast cancer cells from DNA damage-induced apoptosis via activation of survival pathways [8,40].

Based on our results, integrin  $\beta 4$  expression in tumors may act as a biomarker for patient stratification at risk for poor chemotherapy outcomes, and personalized treatment strategies would be warranted. Also, targeting pathways mediated by integrin  $\beta 4$  can enhance chemosensitivity, yielding better results in combination with therapeutic agents like Palbociclib [32,43]. Further studies are needed to fully elucidate the molecular mechanisms whereby chemoresistance is conferred by integrin  $\beta 4$  and to identify intervention targets [44]. In vivo studies will be essential for establishing the rationale for targeting integrin  $\beta 4$  in ovarian cancer. Similarly, our study acknowledges limitations regarding the use of cell lines and organoids, which cannot fully reflect the complexity of the tumor microenvironment.

## 5. Conclusions

In summary, our study suggests that integrin  $\beta 4$  is an important modulator of proliferation and response to Cisplatin in ovarian cancer cell models. Expression of integrin  $\beta 4$  inversely correlates with cell cycle progression; the ability of integrin  $\beta 4$  to enhance the survival of cells undergoing cell cycle arrest contributes to chemoresistance and points to a potential target for improving patient outcomes.

**Supplementary Materials:** The following supporting information can be downloaded at: <https://www.mdpi.com/article/10.3390/cancers17091472/s1>, Figure S1: Organoid quantification in 384-well plates; Figure S2: *ITGB4* mRNA expression versus cell cycle gene expression in PDOs; Figure S3: Uncropped Western blot images corresponding to the blots shown in Figures 3A and 7A.

**Author Contributions:** S.F.: Conceptualization, methodology, validation, software, formal analysis, investigation, data curation, writing—original draft, visualization; D.C.: Methodology, validation, formal analysis, investigation, visualization; J.S.-C.: Conceptualization, methodology, formal analysis, investigation, writing; T.P. (Teagan Polotaye): Methodology, validation, formal analysis, investigation, visualization; T.P. (Tonja Pavlovic): Conceptualization, methodology; P.B.: Methodology, software, formal analysis, visualization; T.M.: Conceptualization, methodology, validation; C.M.: Resources, validation; P.J.: Resources, validation; E.D.: Resources, validation; M.P.Z.: Resources, validation; P.Y.L.: Conceptualization, software; L.A.M.: Conceptualization, methodology, funding acquisition; M.P.I.: Conceptualization, methodology, writing—original draft, visualization, supervision, funding acquisition. All authors have read and agreed to the published version of the manuscript.

**Funding:** This study was supported by NIH/NCI R21CA256615 (M.I.), an Olipass Corporation grant (M.I.), the Kaleidoscope of Hope Ovarian Cancer Research Foundation (M.I.), the New York Stem Cell Foundation Research Institute (NYSCF), the NCI R21CA240219 (L.A.M.), the Polish National Agency for Academic Exchange NAWA STER Program No. PPI/STE/2020/1/00014/DEC/02 (C.M.), statutory funding for young researchers—doctoral students for 2024/25—No 130/2024/DGB (C.M.), and the Foundation for Polish Science First Team Program FENG.02.02-IP.05-0361/23 (M.Z.).

**Institutional Review Board Statement:** Not applicable.

**Informed Consent Statement:** Not applicable.

**Data Availability Statement:** The datasets analyzed in this study include publicly available TCGA transcriptomic data (<https://portal.gdc.cancer.gov/projects/TCGA-OV> (accessed on 14 April 2025)). The original code used for analysis is available at: [https://github.com/pbabwey/cellProliferation\\_matrixAdhesion](https://github.com/pbabwey/cellProliferation_matrixAdhesion). Additional raw data generated during the current study are available from the corresponding author on reasonable request.

**Conflicts of Interest:** Author P.L. owns stocks in the company Auransa.

## References

1. Garsed, D.W.; Pandey, A.; Fereday, S.; Kennedy, C.J.; Takahashi, K.; Alsop, K.; Hamilton, P.T.; Hendley, J.; Chiew, Y.E.; Traficante, N.; et al. The genomic and immune landscape of long-term survivors of high-grade serous ovarian cancer. *Nat. Genet.* **2022**, *54*, 1853–1864. [[CrossRef](#)]
2. Alshehri, S.; Pavlovic, T.; Farsinejad, S.; Behboodi, P.; Quan, L.; Centeno, D.; Kung, D.; Rezler, M.; Lee, W.; Jasinski, P.; et al. Extracellular Matrix Modulates Outgrowth Dynamics in Ovarian Cancer. *Adv. Biol.* **2022**, *6*, e2200197. [[CrossRef](#)]
3. Farsinejad, S.; Cattabiani, T.; Muranen, T.; Iwanicki, M. Ovarian Cancer Dissemination—A Cell Biologist’s Perspective. *Cancers* **2019**, *11*, 1957. [[CrossRef](#)]
4. Hynes, R.O. Integrins: Versatility, modulation, and signaling in cell adhesion. *Cell* **1992**, *69*, 11–25. [[CrossRef](#)]
5. Hynes, R.O. Integrins: Bidirectional, allosteric signaling machines. *Cell* **2002**, *110*, 673–687. [[CrossRef](#)] [[PubMed](#)]
6. Guo, W.; Pylayeva, Y.; Pepe, A.; Yoshioka, T.; Muller, W.J.; Inghirami, G.; Giancotti, F.G. Beta 4 integrin amplifies ErbB2 signaling to promote mammary tumorigenesis. *Cell* **2006**, *126*, 489–502. [[CrossRef](#)] [[PubMed](#)]
7. Muranen, T.; Iwanicki, M.P.; Curry, N.L.; Hwang, J.; DuBois, C.D.; Coloff, J.L.; Hitchcock, D.S.; Clish, C.B.; Brugge, J.S.; Kalaany, N.Y. Starved epithelial cells uptake extracellular matrix for survival. *Nat. Commun.* **2017**, *8*, 13989. [[CrossRef](#)] [[PubMed](#)]

8. Fang, H.; Ren, W.; Cui, Q.; Liang, H.; Yang, C.; Liu, W.; Wang, X.; Liu, X.; Shi, Y.; Feng, J.; et al. Integrin beta4 promotes DNA damage-related drug resistance in triple-negative breast cancer via TNFAIP2/IQGAP1/RAC1. *eLife* **2023**, *12*, RP88483. [\[CrossRef\]](#)
9. Uphoff, C.C.; Drexler, H.G. Detection of mycoplasma contaminations. *Methods Mol. Biol.* **2005**, *290*, 13–23. [\[CrossRef\]](#)
10. Kopper, O.; de Witte, C.J.; Lohmussaar, K.; Valle-Inclan, J.E.; Hami, N.; Kester, L.; Balgobind, A.V.; Korving, J.; Proost, N.; Begthel, H.; et al. An organoid platform for ovarian cancer captures intra- and interpatient heterogeneity. *Nat. Med.* **2019**, *25*, 838–849. [\[CrossRef\]](#)
11. Kessler, M.; Hoffmann, K.; Brinkmann, V.; Thieck, O.; Jackisch, S.; Toelle, B.; Berger, H.; Mollenkopf, H.J.; Mangler, M.; Sehoul, J.; et al. The Notch and Wnt pathways regulate stemness and differentiation in human fallopian tube organoids. *Nat. Commun.* **2015**, *6*, 8989. [\[CrossRef\]](#) [\[PubMed\]](#)
12. Maenhoudt, N.; Defraye, C.; Boretto, M.; Jan, Z.; Heremans, R.; Boeckx, B.; Hermans, F.; Arijs, I.; Cox, B.; Van Nieuwenhuysen, E.; et al. Developing Organoids from Ovarian Cancer as Experimental and Preclinical Models. *Stem Cell Rep.* **2020**, *14*, 717–729. [\[CrossRef\]](#) [\[PubMed\]](#)
13. Sachs, N.; de Ligt, J.; Kopper, O.; Gogola, E.; Bounova, G.; Weeber, F.; Balgobind, A.V.; Wind, K.; Gracanin, A.; Begthel, H.; et al. A Living Biobank of Breast Cancer Organoids Captures Disease Heterogeneity. *Cell* **2018**, *172*, 373–386.e10. [\[CrossRef\]](#)
14. Huber, W.; Carey, V.J.; Gentleman, R.; Anders, S.; Carlson, M.; Carvalho, B.S.; Bravo, H.C.; Davis, S.; Gatto, L.; Girke, T.; et al. Orchestrating high-throughput genomic analysis with Bioconductor. *Nat. Methods* **2015**, *12*, 115–121. [\[CrossRef\]](#) [\[PubMed\]](#)
15. Love, M.I.; Huber, W.; Anders, S. Moderated estimation of fold change and dispersion for RNA-seq data with DESeq2. *Genome Biol.* **2014**, *15*, 550. [\[CrossRef\]](#)
16. Ashburner, M.; Ball, C.A.; Blake, J.A.; Botstein, D.; Butler, H.; Cherry, J.M.; Davis, A.P.; Dolinski, K.; Dwight, S.S.; Eppig, J.T.; et al. Gene ontology: Tool for the unification of biology. The Gene Ontology Consortium. *Nat. Genet.* **2000**, *25*, 25–29. [\[CrossRef\]](#)
17. Kanehisa, M.; Goto, S. KEGG: Kyoto encyclopedia of genes and genomes. *Nucleic Acids Res.* **2000**, *28*, 27–30. [\[CrossRef\]](#)
18. Hanzelmann, S.; Castelo, R.; Guinney, J. GSEA: Gene set variation analysis for microarray and RNA-seq data. *BMC Bioinform.* **2013**, *14*, 7. [\[CrossRef\]](#)
19. Subramanian, A.; Tamayo, P.; Mootha, V.K.; Mukherjee, S.; Ebert, B.L.; Gillette, M.A.; Paulovich, A.; Pomeroy, S.L.; Golub, T.R.; Lander, E.S.; et al. Gene set enrichment analysis: A knowledge-based approach for interpreting genome-wide expression profiles. *Proc. Natl. Acad. Sci. USA* **2005**, *102*, 15545–15550. [\[CrossRef\]](#)
20. Liberzon, A.; Subramanian, A.; Pinchback, R.; Thorvaldsdottir, H.; Tamayo, P.; Mesirov, J.P. Molecular signatures database (MSigDB) 3.0. *Bioinformatics* **2011**, *27*, 1739–1740. [\[CrossRef\]](#)
21. Yu, G.; Wang, L.G.; Han, Y.; He, Q.Y. clusterProfiler: An R package for comparing biological themes among gene clusters. *OMICS* **2012**, *16*, 284–287. [\[CrossRef\]](#) [\[PubMed\]](#)
22. Mootha, V.K.; Lindgren, C.M.; Eriksson, K.F.; Subramanian, A.; Sihag, S.; Lehar, J.; Puigserver, P.; Carlsson, E.; Ridderstrale, M.; Laurila, E.; et al. PGC-1alpha-responsive genes involved in oxidative phosphorylation are coordinately downregulated in human diabetes. *Nat. Genet.* **2003**, *34*, 267–273. [\[CrossRef\]](#) [\[PubMed\]](#)
23. Cancer Genome Atlas Research, N. Integrated genomic analyses of ovarian carcinoma. *Nature* **2011**, *474*, 609–615. [\[CrossRef\]](#) [\[PubMed\]](#)
24. Zeller, T.; Munnich, I.A.; Windisch, R.; Hilger, P.; Schewe, D.M.; Humpe, A.; Kellner, C. Perspectives of targeting LILRB1 in innate and adaptive immune checkpoint therapy of cancer. *Front. Immunol.* **2023**, *14*, 1240275. [\[CrossRef\]](#)
25. Hoshino, A.; Boutboul, D.; Zhang, Y.; Kuehn, H.S.; Hadjadj, J.; Ozdemir, N.; Celkan, T.; Walz, C.; Picard, C.; Lenoir, C.; et al. Gain-of-function IKZF1 variants in humans cause immune dysregulation associated with abnormal T/B cell late differentiation. *Sci. Immunol.* **2022**, *7*, eabi7160. [\[CrossRef\]](#)
26. Jacob, M.; Chang, L.; Pure, E. Fibroblast activation protein in remodeling tissues. *Curr. Mol. Med.* **2012**, *12*, 1220–1243. [\[CrossRef\]](#)
27. Kang, H.C.; Kim, I.J.; Park, J.H.; Shin, Y.; Ku, J.L.; Jung, M.S.; Yoo, B.C.; Kim, H.K.; Park, J.G. Identification of genes with differential expression in acquired drug-resistant gastric cancer cells using high-density oligonucleotide microarrays. *Clin. Cancer Res.* **2004**, *10*, 272–284. [\[CrossRef\]](#)
28. Tsunoda, T.; Koga, H.; Yokomizo, A.; Tatsugami, K.; Eto, M.; Inokuchi, J.; Hirata, A.; Masuda, K.; Okumura, K.; Naito, S. Inositol 1,4,5-trisphosphate (IP3) receptor type1 (IP3R1) modulates the acquisition of cisplatin resistance in bladder cancer cell lines. *Oncogene* **2005**, *24*, 1396–1402. [\[CrossRef\]](#)
29. Whiteside, M.A.; Chen, D.T.; Desmond, R.A.; Abdulkadir, S.A.; Johanning, G.L. A novel time-course cDNA microarray analysis method identifies genes associated with the development of cisplatin resistance. *Oncogene* **2004**, *23*, 744–752. [\[CrossRef\]](#)
30. Stewart, R.L.; O'Connor, K.L. Clinical significance of the integrin alpha6beta4 in human malignancies. *Lab. Invest.* **2015**, *95*, 976–986. [\[CrossRef\]](#)
31. Asghar, U.; Witkiewicz, A.K.; Turner, N.C.; Knudsen, E.S. The history and future of targeting cyclin-dependent kinases in cancer therapy. *Nat. Rev. Drug Discov.* **2015**, *14*, 130–146. [\[CrossRef\]](#) [\[PubMed\]](#)



32. Finn, R.S.; Crown, J.P.; Lang, I.; Boer, K.; Bondarenko, I.M.; Kulyk, S.O.; Ettl, J.; Patel, R.; Pinter, T.; Schmidt, M.; et al. The cyclin-dependent kinase 4/6 inhibitor palbociclib in combination with letrozole versus letrozole alone as first-line treatment of oestrogen receptor-positive, HER2-negative, advanced breast cancer (PALOMA-1/TRIO-18): A randomised phase 2 study. *Lancet Oncol.* **2015**, *16*, 25–35. [\[CrossRef\]](#)
33. Thangavel, C.; Boopathi, E.; Liu, Y.; Haber, A.; Ertel, A.; Bhardwaj, A.; Addya, S.; Williams, N.; Ciment, S.J.; Cotzia, P.; et al. RB Loss Promotes Prostate Cancer Metastasis. *Cancer Res.* **2017**, *77*, 982–995. [\[CrossRef\]](#) [\[PubMed\]](#)
34. Knudsen, E.S.; Witkiewicz, A.K. The Strange Case of CDK4/6 Inhibitors: Mechanisms, Resistance, and Combination Strategies. *Trends Cancer* **2017**, *3*, 39–55. [\[CrossRef\]](#) [\[PubMed\]](#)
35. Thura, M.; Al-Aidaroos, A.Q.; Gupta, A.; Chee, C.E.; Lee, S.C.; Hui, K.M.; Li, J.; Guan, Y.K.; Yong, W.P.; So, J.; et al. Author Correction: PRL3-zumab as an immunotherapy to inhibit tumors expressing PRL3 oncoprotein. *Nat. Commun.* **2021**, *12*, 6431. [\[CrossRef\]](#)
36. Domcke, S.; Sinha, R.; Levine, D.A.; Sander, C.; Schultz, N. Evaluating cell lines as tumour models by comparison of genomic profiles. *Nat. Commun.* **2013**, *4*, 2126. [\[CrossRef\]](#)
37. Cocco, E.; Scaltriti, M.; Drilon, A. NTRK fusion-positive cancers and TRK inhibitor therapy. *Nat. Rev. Clin. Oncol.* **2018**, *15*, 731–747. [\[CrossRef\]](#)
38. Zhang, J.; Xu, K.; Liu, P.; Geng, Y.; Wang, B.; Gan, W.; Guo, J.; Wu, F.; Chin, Y.R.; Berrios, C.; et al. Inhibition of Rb Phosphorylation Leads to mTORC2-Mediated Activation of Akt. *Mol. Cell* **2016**, *62*, 929–942. [\[CrossRef\]](#)
39. Mercurio, A.M.; Bachelder, R.E.; Bates, R.C.; Chung, J. Autocrine signaling in carcinoma: VEGF and the alpha6beta4 integrin. *Semin Cancer Biol.* **2004**, *14*, 115–122. [\[CrossRef\]](#)
40. Bandyopadhyay, A.; Wang, L.; Agyin, J.; Tang, Y.; Lin, S.; Yeh, I.T.; De, K.; Sun, L.Z. Doxorubicin in combination with a small TGFbeta inhibitor: A potential novel therapy for metastatic breast cancer in mouse models. *PLoS ONE* **2010**, *5*, e10365. [\[CrossRef\]](#)
41. Bierie, B.; Pierce, S.E.; Kroeger, C.; Stover, D.G.; Pattabiraman, D.R.; Thiru, P.; Liu Donaher, J.; Reinhardt, F.; Chaffer, C.L.; Keckesova, Z.; et al. Integrin-beta4 identifies cancer stem cell-enriched populations of partially mesenchymal carcinoma cells. *Proc. Natl. Acad. Sci. USA* **2017**, *114*, E2337–E2346. [\[CrossRef\]](#) [\[PubMed\]](#)
42. Florea, A.M.; Busselberg, D. Cisplatin as an anti-tumor drug: Cellular mechanisms of activity, drug resistance and induced side effects. *Cancers* **2011**, *3*, 1351–1371. [\[CrossRef\]](#) [\[PubMed\]](#)
43. Turner, N.C.; Huang Bartlett, C.; Cristofanilli, M. Palbociclib in Hormone-Receptor-Positive Advanced Breast Cancer. *N. Engl. J. Med.* **2015**, *373*, 1672–1673. [\[CrossRef\]](#) [\[PubMed\]](#)
44. Courtney, K.D.; Corcoran, R.B.; Engelman, J.A. The PI3K pathway as drug target in human cancer. *J. Clin. Oncol.* **2010**, *28*, 1075–1083. [\[CrossRef\]](#)

**Disclaimer/Publisher’s Note:** The statements, opinions and data contained in all publications are solely those of the individual author(s) and contributor(s) and not of MDPI and/or the editor(s). MDPI and/or the editor(s) disclaim responsibility for any injury to people or property resulting from any ideas, methods, instructions or products referred to in the content.